

POLITECNICO DI TORINO

Master degree course in "Ingegneria Energetica e Nucleare"

Master Degree Thesis

**Numerical model of a carbonator  
reactor for thermochemical energy  
storage based on Calcium Looping**



**Supervisors:**

prof. Vittorio Verda

dott. ing. Elisa Guelpa

**Candidate**

Gianfranco CAFORIO

matricola: 240949

ANNO ACCADEMICO 2017/2018

This work is subject to the Creative Commons Licence

# Acknowledgements

Thanks to my family, which has always believed in me in these years, with love and unconditional support.

Thanks to all my friends, who helped me to forget about the university problems and without which I would not arrived so far, and all my colleagues, with which I passed happy and anxious moments, and with which I grew up in these years.

Thanks to my supervisors, Vittorio Verda and Elisa Guelpa, who guided me in this ambitious work.

*You can never cross the ocean unless  
you have the courage to lose sight of the  
shore.*

[DAVID L. WEATHERFORD]

# Abstract

In the landscape of the renewable energy power plant the Concentrated Solar Power plants should play a leading role in the near future. To overcome the known problem of the intermittence, different kind of energy storage are developed during the years. The most promising technologies, in terms of long-term storage and energy density, are the so called Thermochemical Energy Storage, and the Ca-looping, which uses the exothermic reaction between CaO and CO<sub>2</sub>, is nowadays one of them in the development phase. The carbonator and the calciner are the two reactors which compose the Ca-looping, where the exothermic and the endothermic reactions take place, respectively.

After a first introduction about the Ca-looping, the fluidized bed reactor technology, and the ideal reactors, a carbonator numerical model is introduced, starting from the study of the application in CO<sub>2</sub> capture plant. The model is divided in three main sub-models: hydrodynamic, based on Kunii-Levenspiel model, chemistry, based on a perfectly mixed model for the solid phase and a plug flow for the gas phase, and energy, which uses a cluster renewal model to study the heat transfer in the reactor. After that, the model, implemented on Matlab, is verified against the available data in literature as carbonator for the CO<sub>2</sub> capturing, and it is adjusted for the use in a Thermochemical Energy Storage technology. Finally, thanks to the energy model introduced, membrane walls are planned in the reactor, in order to extract heat with a coolant, and to use it in a external thermodynamic cycle. In conclusion, the effects of the design variables and of the operating conditions on the output results are studied.

# Abstract

Nel panorama delle energie rinnovabili, gli impianti termodinamici a concentrazione solare puntano a coprire un ruolo da protagonista nel mercato energetico del prossimo futuro. Per risolvere il ben noto problema dell'intermittenza nella produzione, diversi tipi di accumuli energetici sono stati sviluppati durante gli anni. La tecnologia più promettente, grazie alla possibilità di accumulo a lungo termine e all'elevata densità energetica, è basata sull'accumulo termochimico, e, in particolare, il loop del calcio, che utilizza la reazione esotermica tra  $\text{CaO}$  e  $\text{CO}_2$ , è attualmente uno dei più promettenti tipi di accumulo termochimico, ma ancora nella sua fase di sviluppo. Il loop del calcio è basato fondamentalmente su due reattori chimici, il reattore di carbonatazione e il reattore di calcinazione, dove le reazioni esotermiche ed endotermiche hanno luogo rispettivamente.

Dopo una prima parte introduttiva incentrata sul loop del calcio, sulla tecnologia dei reattori a letto fluido, e sulla modellazione di reattori chimici ideali, il presente lavoro verte sulla presentazione di un modello numerico del reattore di carbonatazione, partendo dallo studio di carbonatori utilizzati per la cattura di  $\text{CO}_2$ . Il modello numerico proposto è divisibile in tre sottomodelli, ognuno dei quali tratta un differente aspetto del reattore: modello idrodinamico, basato sul modello Kunii-Levenspiel, modello chimico, basato sulla modellazione della fase gassosa come plug-flow e della fase solida come perfettamente miscelata, e modello energetico, basato sul modello di rinnovo dei cluster (*cluster renewal model*). In seguito, il modello implementato in Matlab, e verificato rispetto ai dati di funzionamento pubblicati in letteratura per applicazioni di cattura di  $\text{CO}_2$ , è applicato alle particolari condizioni della tecnologia di accumulo. Grazie al modello energetico introdotto, il possibile utilizzo di pareti membranate, utili per rimuovere calore del reattore per il funzionamento di un motore Stirling esterno, è stato valutato, ed in conclusione gli effetti delle variazioni delle condizioni operative e dei parametri di progetto sono stati analizzati.

# List of Figures

1.1	Energy density of different energy storage technologies as a function of the temperature needed [1] . . . . .	3
2.1	Scheme of the Ca-Looping plant for CO <sub>2</sub> capture [13] . . . . .	6
2.2	Schematic representation of the CaL-CSP integrated with a CO <sub>2</sub> closed Brayton cycle [14] . . . . .	7
2.3	Gas and solid mass flow rate in the plant between carbonator and calciner [14] . . . . .	8
2.4	Thermogravimetric analysis for the first carbonation cycle, for particles with diameter smaller than 45 $\mu m$ , under TCES conditions (a) and CO <sub>2</sub> condtions (b) [7] . . . . .	10
2.5	Multicycle activity of dolomite and limestone for CaL-CO <sub>2</sub> capture conditions and for CaL-CSP conditions for particle diameter smaller than 45 $\mu m$ . . . . .	10
3.1	Contactig regimes [4] . . . . .	13
3.2	Turbulent fluidized bed (a), fast fluidized bed (b) [4] . . . . .	14
3.3	Cross sectional view of a cyclone [31] . . . . .	15
3.4	Standpipe-loop seal arrangement [9] . . . . .	16
3.5	Classification of solids depending on their behavior when fluidized [4] . . . . .	17
3.6	Map regime diagram of fluidized beds [11] . . . . .	18
3.7	Sketch of a fast fluidized regime [31] . . . . .	19
4.1	Representation of the contact regime in a batch reactor [15] . . . . .	21
4.2	Representation of the contacting pattern in a CSTR [15] . . . . .	23
4.3	Mole balance applied to a finite volume for the species j in a PFR [15] . . . . .	24
4.4	Scheme of a PBR . . . . .	25
5.1	Concept diagram of the carbonator model . . . . .	27

5.2	Sketch of the pattern in a fast fluidized regime reactor, on the left [21], and the exponential decay model of the solid volumetric fraction, on the right . . . . .	29
5.3	Sketch of the core/annulus model used [22] . . . . .	31
5.4	Sorbent conversion vs number of cycles for a typical CO <sub>2</sub> capture application . . . . .	33
5.5	Schematic representation of the calcium looping system [24] in a CaL-CO <sub>2</sub> capture plant . . . . .	33
5.6	Moles of CO <sub>2</sub> transported with partial conversion or with maximum carbonation/calcination conversion as a function of N [27] . . . . .	35
5.7	Fraction of CaO in the cycle $N$ , or $N_{age}$ , for different partial carbonation levels . . . . .	36
5.8	Typical profile of the pdf of the particles residence time . . . . .	37
5.9	Equilibrium CO <sub>2</sub> pressure based on eqn. (5.21) . . . . .	38
5.10	Equivalent electrical circuit of the carbon dioxide reaction, to go from the reactants to the products . . . . .	40
5.11	Carbonated particles fraction as a function of time parameterized for different carbonation cycles and equivalent CO <sub>2</sub> concentration at which it is exposed . . . . .	43
5.12	Classification of the heat transfer models . . . . .	46
5.13	Representation of the cluster renewal model, (vijay and reddy 2005) . . . . .	47
5.14	Typical values of the local heat transfer coefficient as a function of the height . . . . .	51
5.15	Representation of the cross section of the membrane wall used and of the portion analyzed (shaded) [23] . . . . .	52
5.16	Membrane wall geometric parameters and heat transfer coefficients [23] . . . . .	53
5.17	Equivalent thermal circuit for the heat transfer from the bed to the coolant . . . . .	53
5.18	Equivalent thermal circuit with internal and external fins . . . . .	54
5.19	Energy balance applied on the carbonator reactor . . . . .	55
5.20	Flow chart of the carbonator model . . . . .	58
5.21	Output results from the model proposed by Romano in [24] compared with respect to the data from the INCAR-CSIC carbonator on the left, and with the data from IFK carbonator on the right [44] . . . . .	59
6.1	Results from the geometrical optimization of the internal fins, with Re of the coolant of $\sim 2'000$ . . . . .	61
6.2	Cross-sectional view of the tube composing the membrane walls . . . . .	62
6.3	Solid fraction profile (a), temperature of the coolant as a function of z (b) using reference design variables and operating conditions . . . . .	63

6.4	Carbonator scheme, using reference operating conditions and design variables . . . . .	63
6.5	a) Sorbent carbonation degree ( $CO_2 = 11.24 mol/m^3, N = 100$ ), b) limit time as a function of $C_{CO_2}$ ( $N=100, T_{bed} = 832 \text{ }^\circ\text{C}$ ) . . . . .	65
6.6	Partial carbonation as a function of different average residence times in the reactor for carbonator in TCES ( $p=1 \text{ bar}$ ) and in $CO_2$ capture plant ( $p_{CO_2}=0.2 \text{ bar}$ ) . . . . .	65
6.7	Solid fraction profiles for different reactor diameters (a), heat transfer coefficient, bed side, and total coolant mass flow rate for different reactor diameters (b) . . . . .	66
6.8	Logarithmic mean value of the local heat transfer coefficient in the reactor as a function of the reactor diameter (a), power released and power extracted as a function of the reactor diameter (b) . . . . .	67
6.9	Solid fraction profiles for different reactor total height (a), Logarithmic mean value of the heat transfer coefficient, bed side, as a function of the reactor height (b) . . . . .	68
6.10	Sensitivity analysis of the carbonator model with respect to the variation of the recycling rate . . . . .	68
6.11	Power released and extracted as a function of the make-up flow in the carbonator (a), bed temperature as a function of the make-up flow (b) with reference design variables and operating conditions . . . . .	69
6.12	Average carbonation degree of the particles in the carbonator as a function of the make-up flow . . . . .	70
6.13	Average carbonation degree of the particles in the carbonator as a function of the make-up flow, using reference design variables and operating conditions, with pressure of the reactor equal to 1, 2 and 3 bar . . . . .	70
6.14	Bed temperature (a) and power released by the exothermic reaction (b) as a function of the ratio $F_0/F_{CO_2}$ . . . . .	71

# Contents

<b>Acknowledgements</b>	III
<b>1 Introduction</b>	1
1.1 Energy storage	2
1.2 Aim of the work	4
<b>2 Ca-looping</b>	5
2.1 Ca-loop for TCES	6
2.2 CaO carbonation behavior in the Ca-Loop	9
<b>3 Fluidized bed</b>	12
3.1 Gas-solid contacting regime	12
3.1.1 Cyclone	14
3.1.2 Standpipe-loop seal	15
3.2 Geldart particles classification	16
3.3 Mapping of fluidization regimes	17
3.4 Circulating fluidized bed	17
<b>4 Ideal models for chemical reactors</b>	20
4.1 Batch reactors	21
4.2 Continuous flow reactor	22
4.2.1 Continuous-stirred tank reactor (CSTR)	22
4.2.2 Plug-flow reactor (PFR)	23
4.2.3 Packed bed reactor (PBR)	24
<b>5 Carbonator numerical model</b>	26
5.1 Hydrodynamic model	27
5.1.1 Kunii and Levenspiel model	27
5.1.2 Core/annulus model	30
5.2 CaO carbon capture capacity	32
5.2.1 Partial carbonation/calcination	34

5.2.2	Particles residence time . . . . .	37
5.3	Gas kinetic model . . . . .	38
5.4	Solid kinetic model . . . . .	41
5.5	Heat transfer model . . . . .	44
5.5.1	Cluster renewal model . . . . .	46
5.5.2	Membrane walls and energy balance . . . . .	51
5.6	Algorithm . . . . .	55
<b>6</b>	<b>Data and results</b>	<b>60</b>
6.1	Reference design variables and operating conditions . . . . .	60
6.2	Analysis of the results for different input values . . . . .	64
6.2.1	Effect of diameter variation . . . . .	65
6.2.2	Effect of reactor total height variation . . . . .	67
6.2.3	Effect of $F_R$ variation . . . . .	67
6.2.4	Effect of $F_0$ variation . . . . .	69
<b>7</b>	<b>Conclusions</b>	<b>72</b>
	<b>Bibliography</b>	<b>74</b>

# Nomenclature

## Abbreviations

BFB Bubbling Fluidized Bed

CaL-CO<sub>2</sub> Ca-looping applied used as Carbon Capture Storage technology

CaL-CSP Ca-looping applied as Thermochemical Energy Storage in Concentrated Solar Power plant

CFB Circulating Fluidized Bed

K-L Kunii-Levenspiel

PCM Phase Change Material

TCES Thermochemical Energy Storage

TES Thermal Energy Storage

TFB Turbulent fluidized bed

TGA Thermogravimetric analyzer

## Greek symbols

$\delta_d, \delta_l$  volumetric fraction of core in the bottom dense region and in top lean region [-]

$\epsilon$  local void fraction in the reactor [-]

$\eta_d, \eta_l$  contact efficiency in the dense and lean region [-]

$\rho_c$  density of the clusters [ $kg/m^3$ ]

$\rho_s$  solid density [ $kg/m^3$ ]

$\rho_g$  gas density [ $kg/m^3$ ]

---

$\rho_{susp}$	suspension density in the reactor [ $kg/m^3$ ]
$\sigma$	Stefan-Boltzmann constant [ $W/(mK^{-4})$ ]
$\tau$	particle average residence time [ $s$ ]

### Latin symbols

$a$	solid concentration decay constant in the lean region [ $m^{-1}$ ]
$\delta$	dimensionless gas layer thickness [-]
$\dot{m}_{g,in}$	gas mass flow rate entering the reactor [ $kg/s$ ]
$\dot{m}_{g,out}$	gas mass flow rate exiting the reactor [ $kg/s$ ]
$\dot{m}_{s,in}$	solid mass flow rate entering the reactor [ $kg/s$ ]
$\dot{m}_{s,out}$	solid mass flow rate exiting the reactor [ $kg/s$ ]
$\epsilon_c$	void in the clusters [-]
$\eta_{ext,fin}$	efficiency of the external fins [-]
$\eta_{int,fin}$	efficiency of the internal fins [-]
$\rho_d$	density of the dilute phase [ $kg/m^3$ ]
$A_t$	cross section area [ $m^2$ ]
$A_{ext,fin}$	area of the external fins exposed to the bed [ $m^2$ ]
$A_{int,fin}$	area of the internal fins exposed to the heat transfer fluid [ $m^2$ ]
$c_c$	clusters specific heat [ $KJ/(kg \cdot K)$ ]
$c_{p,g}$	gas specific heat [ $W/(m^2K)$ ]
$c_{p,s}$	solid specific heat [ $W/(m^2K)$ ]
$c_{sf}$	solid fraction of clusters [-]
$CO_{2,eq}$	$CO_2$ concentration at the equilibrium condition defined by $p_{CO_2}$ [ $mol/m^3$ ]
$CO_{2,in}, CO_{2,d}, CO_{2,ex}$	$CO_2$ concentration in inlet, exiting the dense region and exiting the reactor [ $mol/m^3$ ]
$d_p^*$	dimensionless particles diameter [-]
$e_c$	cluster emissivity [-]

---

$e_d$	emissivity of the dilute phas [-]
$e_w$	wall emissivity [-]
$f$	solid volumetric fraction [ $m^3_{solid}/m^3_{reactor}$ ]
$f^*$	solid volumetric fraction in saturated carrying capacity conditions [ $m^3_{solid}/m^3_{reactor}$ ]
$F_0$	calciner make-up molar flow rate [ $kmol/s$ ]
$f_d$	dense region solid volumetric fraction [ $m^3_{solid}/m^3_{reactor}$ ]
$f_l$	solid volumetric fraction [ $m^3_{solid}/m^3_{reactor}$ ]
$f_l$	solid volumetric fraction in the lean region [ $m^3_{solid}/m^3_{reactor}$ ]
$F_R$	carbonator/calciner circulating molar flow rate [ $kmol/s$ ]
$f_t$	probability density function of the sorbent permanence time in the carbonator [-]
$f_{calc}$	average calcination level in the calciner [-]
$f_{carb}$	average carbonation level in the carbonator [-]
$f_{dc}, f_{lc}$	solid volumetric fraction of the core-dense region and of the core-lean region [ $m^3_{solid}/m^3_{reactor}$ ]
$f_{lw}, f_{dw}$	solid volumetric fraction of the wall-lean region and wall-dense region [ $m^3_{solid}/m^3_{reactor}$ ]
$f_{se}$	solid volumetric fraction at the outlet of the reactor [ $m^3_{solid}/m^3_{reactor}$ ]
$f_{w,c}$	fraction of wall covered by clusters [-]
$G_s$	mass velocity [ $kg/(m^2s)$ ]
$H_d$	dense region height [ $m$ ]
$H_l$	lean region height [ $m$ ]
$h_o$	heat transfer coefficient bed side [ $W/(m^2K)$ ]
$H_t$	total height of the reactor [ $m$ ]
$h_c$	cluster thermal resistance [ $W/(m^2K)$ ]
$h_g$	dilute phase thermal resistance [ $W/(m^2K)$ ]
$h_i$	heat transfer coefficient coolant side [ $W/(m^2K)$ ]

---

$h_p$	particles convection heat transfer coefficient [ $W/(m^2K)$ ]
$h_{rc}$	cluster radiative thermal resistance [ $W/(m^2K)$ ]
$h_{rd}$	dilute phase radiative thermal resistance [ $W/(m^2K)$ ]
$h_w$	wall thermal resistance [ $W/(m^2K)$ ]
$k$	kinetic constant of the CaO carbonation reaction and average kinetic constant of the population of the potentially active Ca-based particles, respectively [ $s^{-1}$ ]
$k_c$	thermal conductivity of clusters [ $W/(m^2K)$ ]
$k_r$	kinetic constant of the CaO carbonation reaction [ $m^3/mol/s$ ]
$k_{deact}$	sorbent deactivation constant [-]
$k_t$	conductive heat transfer coefficient of the membrane walls [ $W/(m^2K)$ ]
$L_c$	clusters contact length [ $m$ ]
$N$	number of full carbonation/calcination [-]
$N_{age}$	equivalent number of full carbonation/calcination cycles [-]
$N_{ext,fin}$	number of external fins [-]
$N_{int,fin}$	number of internal fins [-]
$n_{s,a}$	moles of active sorbent particles in the carbonator [ $mol$ ]
$p$	carbonator pressure
$p_c$	coolant pressure
$p_{CO_2,eq}$	equilibrium carbon dioxide pressure in carbonation reaction [ $bar$ ]
$q_{gen}$	power released by the exothermic reaction [ $MW$ ]
$q_{out}$	power extracted from the reactor [ $MW$ ]
$r_N$	fraction of sorbent particles which have experienced N complete carbonation/calcination cycles [-]
$R_{in}$	internal radius of the tube composing the membrane walls [ $m$ ]
$r_{N,age}$	fraction of sorbent particles that have experienced $N_{age}$ equivalent carbonation/calcination cycles [-]

---

$R_{out}$	external radius of the tube composing the membrane walls [ $m$ ]
$R_{tot}(z)$	total thermal resistance bed/heat transfer fluid, as a function of the height [ $W/(m^2K)$ ]
$t$	time [ $s$ ]
$t_c$	contact time of the clusters [-]
$T_w$	reactor walls temperature [ $K$ ]
$T_{bed}$	working temperature of the reactor [ $K$ ]
$T_{c,in}$	inlet temperature of the coolant [ $K$ ]
$T_{c,out}$	outlet temperature of the coolant [ $K$ ]
$T_c(z)$	temperature of coolant as a function of the height in the reactor [ $K$ ]
$T_{g,in}$	inlet temperature of the gas phase [ $K$ ]
$t_{lim}$	limit time for a particles that ends the fast reaction stage [ $s$ ]
$T_{s,in}$	outlet temperature of the solid phase [ $K$ ]
$T_{t,in}$	temperature of inlet surface of the tube composing the membrane walls [ $K$ ]
$T_{t,out}$	temperature of outlet surface of the tube composing the membrane walls [ $K$ ]
$u^*$	dimensionless gas velocity [-]
$u_0$	superficial gas velocity [ $m/s$ ]
$u_g$	gas velocity [ $m/s$ ]
$u_s$	solid velocity [ $m/s$ ]
$u_t$	terminal velocity characteristic of the particle [-]
$U_c$	clusters falling velocity [ $m/s$ ]
$W_d$	dense region solid inventory [ $kg$ ]
$W_l$	lean region solid inventory [ $kg$ ]
$W_s$	solid inventory in the reactor [ $kg$ ]
$X_r$	residual conversion capacity available when N goes to infinity [-]

- $X_{carb}(t)$  carbonation degree of lime (sorbent) particles as a function of time [-]
- $X_{max,ave}$  maximum average activity of the sorbent particles in the reactor [-]
- $X_{max,N}$  maximum carbonation degree after N complete carbonation/calcination cycles [-]
- $Y$  dilute phase solid fraction [-]
- $z$  reactor axial coordinate [m]
- $z_l$  reactor axial coordinate above the dense bed [m]

# Chapter 1

## Introduction

The needs of energy in every day life is a problem that humans dealt since still very early date. The evolution during the centuries brought the building of huge production power plants to fulfill the energy demand, always bigger in size and more complex in the operating principles, where different sources have been used. The most used energy sources nowadays are still fossil fuels, which, unavoidably, bring to the production of carbon dioxide and the environment pollution due to production of ashes, NOx and SOx.

The increasing in CO<sub>2</sub> concentration in the atmosphere, during the years, modified the weather conditions on the earth, increasing the average atmosphere temperature due to the increasing in the green-house effect.

Another problem related with the use of fossil fuels is the their limited quantities, which forced, and is still forcing, the people to find more complex way of their extraction from the ground, trying to use as much as possible sources available on the earth.

In this landscape, the need of a turning point is evident and the most easy solution is to increase the penetration, in the energy market, of renewable energy sources, that can reduce the use of fossil fuel mainly for building energy consumption, but also part of automotive energy demand.

Among the different possibilities, solar energy seems to be the most promising one. The intermittence is the most important problem related with the use of

renewable sources, and in particular with the use of solar thermal power plants, which doesn't allow a constant energy production, and usually is not predictable. The extension of the electrical network could be a solution, but the energy storage seems to be the best and easiest way to overcome this problem.

## 1.1 Energy storage

Energy storage are used to reduce the mismatch between energy supply and energy demand, and so, to reduce the wastefulness of resources. In solar thermal power plant, there are different viable ways to store energy depending on the thermodynamic principle that is used.

In Thermal Energy Storage (TES), the easiest in operating principle, an Heat Transfer Fluid (HTF) is heated up when there is a surplus of energy. Typically the most used HTFs are water, molten salts or thermal oils.

The surplus of energy can be also stored as sensible heat, with a solid/liquid phase transition in the Phase Change Material (PCM) storages.

Storage which use the surplus of energy to carry out an endothermic reaction, and so, storing the energy in the products as chemical energy, are called Thermochemical Energy Storage (TCES).

Among these three possibilities TES and PCM technologies are already installed in plants of considerable size, but they have disadvantages that can not be overcome, as the low value of energy density or the energy losses to the environment, due to the high storing temperature.[\[1\]](#)

From this point of view, the TCES represents a promising possibility, since the products, driven by the endothermic reaction, can be stored at ambient temperature for long terms, and also they make available higher energy density than the TES or PCM, as it can be seen from [Fig. 1.1](#).

There are different endothermic reactions that can be suitable for TCES systems, but one of the most promising, due to its trade off between turning temperature and energy density available, is the Calcium Looping process, which deals with the theoretical reversible carbonation reaction of the lime, or calcium oxide, CaO, reported in eqn. [\(1.1\)](#), whose heat of reaction at reference temperature is  $\Delta H_r^0 = 178kJ/mol$  [\[2\]](#).

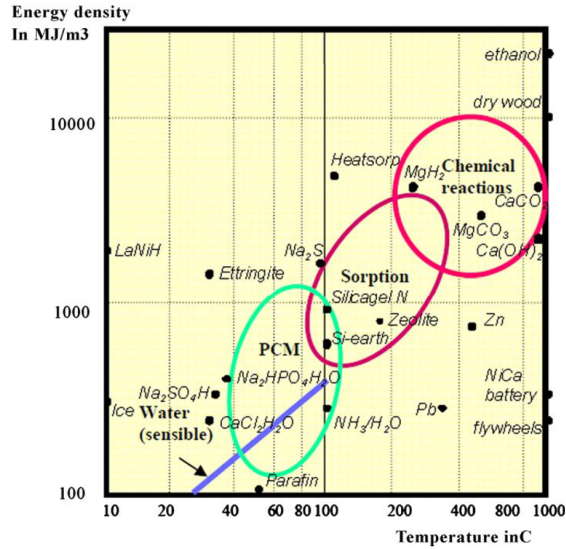


Figure 1.1: Energy density of different energy storage technologies as a function of the temperature needed [1]



A TCES Ca-loop based, would use the heat in the solar peak hours to develop the endothermic reaction of calcination, from calcium carbonate to calcium oxide and carbon dioxide, in a reactor called calciner, storing the product separately. In the night-time, or cloudy hours, the products will react again, with the carbonation of CaO in the carbonator, releasing the heat of reaction.

Calcium loop is a technology already studied and tested in many lab-scale plants as a technology for the CO<sub>2</sub> capture from flue gases. The operating principle is almost the same, and it will be explained in detail during the work. The differences between the use of a Ca-loop as a CCS than TCES are the working conditions, pressure and temperature, of two components, carbonator and calciner. This differences will bring advantages in this application, which is an other promoting aspect of using this technology as a TCES.

## 1.2 Aim of the work

The aim of this work is to develop a numerical model of a carbonator reactor for a TCES ca-loop based, starting from the information available in literature, which is able to predict the hydrodynamic conditions, the CO<sub>2</sub> capture performance, and the energy available in the reactor as a function of the design parameters and operating conditions. Subsequently, the possibility of installing heat transfer surfaces to extract heat from the reactor, that will be used in a Stirling cycle, is studied using the numerical energy model introduced.

## Chapter 2

# Ca-looping

The Ca-Loop is a chemical loop born mainly as a CO<sub>2</sub> carbon capture storage technology (CCS). It is based on the idea to use lime (CaO), to remove CO<sub>2</sub> from the flue gasses exiting coal fired power plants, thus, as a post-combustion capture technology, producing a pure stream of CO<sub>2</sub> to store, and calcium carbonate (CaCO<sub>3</sub>).

The Ca-Loop is composed by a calciner, a chemical reactor in which the CaO precursor is decomposed by endothermic reaction in CaO and CO<sub>2</sub>, and a carbonator, a chemical reactor in which CaO and CO<sub>2</sub> react again releasing energy in an exothermic reaction. A scheme of the Ca-Loop for CCS application is reported in Fig. 2.1.

As it can be seen from Fig. 2.1, to carry out the endothermic calcination reaction, the calciner is fed by fuel, which burns typically under oxyfuel conditions, namely with pure oxygen, with production of ash.

In a CaL-CO<sub>2</sub> capture integration, the typical working temperature of the calciner is 900°C, under atmosphere of pure CO<sub>2</sub>, and of the carbonator is 650°C, under poor atmosphere of CO<sub>2</sub>. These conditions are mainly justified by the fact that the carbonation reaction of lime is an equilibrium reaction, and so, the reaction direction depends on the temperature and partial pressure of CO<sub>2</sub> in which it takes place. Furthermore, since it is an equilibrium reaction in a continuous flow working conditions, it will never reach 100% capture efficiency but, in any case,

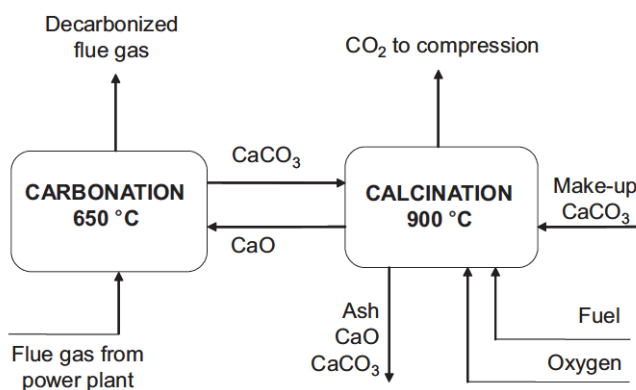


Figure 2.1: Scheme of the Ca-Looping plant for CO<sub>2</sub> capture [13]

efficiency of 80%-90% are considered cost effective for CCS.

The main aspect whereby the Ca-Loop is become the most promising technology for CCS is the advantage of the CaO precursor used: the limestone. It is an abundant non-toxic and non corrosive cheap material, which costs almost 10 \$/ton, geographically widespread. Furthermore, during the years, it reached the largest progress in technology readiness level [3] due to its similarity in the reactors technology, based on existing combustion circulating fluidized beds. Of course all these advantages will be valid when the Ca-Loop is used as TCES as well.

## 2.1 Ca-loop for TCES

The intermittent availability of renewable energy sources, and possibility of storage and delivering phase decoupled given by the Ca-Looping, can be combined in a Thermochemical Energy Storage technology. This idea comes from 30 years ago, and nowadays SOCRATCES, an European project, is aimed at demonstrating the feasibility of this CaL-CSP technology erecting a pilot-scale plant, using solar tower plant which can operate at higher temperature than parabolic linear systems.

The cycle starts in the calciner where the calcination reaction takes place using the solar energy. The reaction is performed in a solar reactor, placed in a central tower receiver working at almost 700°C (much lower than CaL-CO<sub>2</sub> capture temperatures) under atmosphere of Helium or superheated steam, that are gasses easily

separable from  $\text{CO}_2$ , that enhance heat transfer and  $\text{CO}_2$  diffusivity increasing the reaction kinetics, and that allow to reduce the calcination temperature.

Once calcination is completed and the gasses are extracted, the  $\text{CO}_2$  is cooled down, compressed and sent into a storage, whereas the  $\text{CaO}$  is cooled to ambient temperature and stored in a solid reservoir.

The energy discharging phase takes place in the carbonator, which is a pressurized fluidized bed working in fast fluidization regime and at temperature slightly higher than  $850^\circ\text{C}$ . The heat from the reaction can be delivered directly with the reactant ( $\text{CO}_2$ ) that have not been captured, or using heat exchanger surfaces in the carbonator, using the energy removed in an external thermodynamic cycles, such as a Stirling cycle. The exiting solids, composed by  $\text{CaCO}_3$  and  $\text{CaO}$  that have not reacted, is sent to a solid storage. A schematic representation of the CaL-CSP technology is reported in Fig. 2.2.

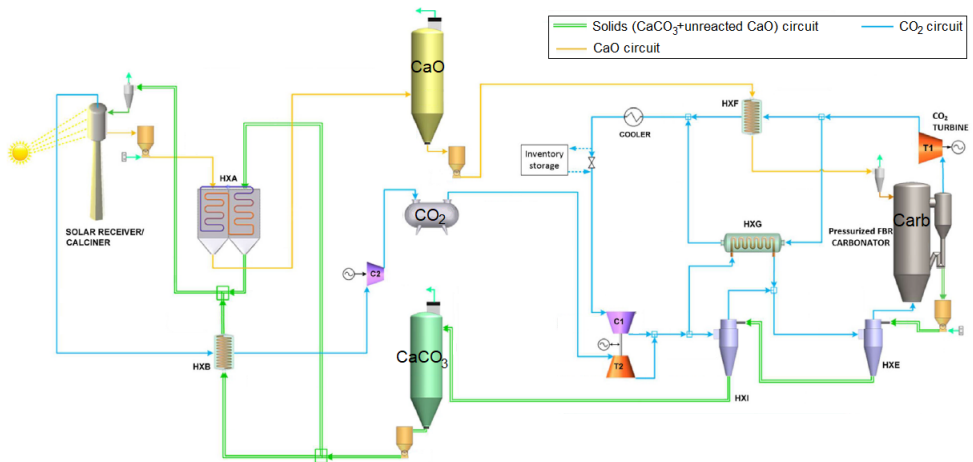


Figure 2.2: Schematic representation of the CaL-CSP integrated with a  $\text{CO}_2$  closed Brayton cycle [14]

Furthermore, in order to achieve higher integration efficiency, an heat exchangers network has been designed in [14], using gas-gas regenerators, gas-solid cyclone heat exchangers and solid-solid heat exchangers. The gas-solid heat exchanger used operates in counter-flow and consists in a series of vertical plates, in which the gas flows, across which bulk solids flow downwards exchanging heat. Adapting this

technology using one or more intermediate heat transfer fluid, also the solid-solid heat exchange can be pursued.

The flows circulating in carboantor and calciner regions are separated, due to the storages that are filled and emptied in different moment, or with different rate. While the calciner can work only if there is enough solar power, the carbonator must satisfied a 24 hours period of power demand, thus the storage vessel must be sized in order to guarantee demand over the day [14]. Fig. 2.3 reports the mass flows in these two regions of the plant. If it is considered average working conditions, with day averaged molar flows, and the daytime period in which the decomposition temperature is reached in the calciner,  $\Delta t_{sun}$ , it is possible to derive an average ratio between between circulating flow rates in the calciner and in the carbonator [14]:

$$\overline{F_{CaCO_3,clc}} \Delta t_{sun} = \overline{F_{CaCO_3,crb}} 24 \quad (2.1)$$

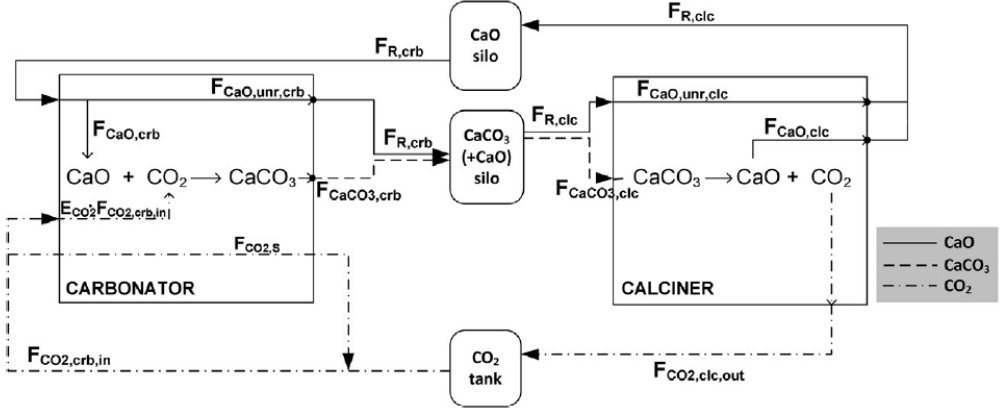


Figure 2.3: Gas and solid mass flow rate in the plant between carbonator and calciner [14]

It is a usual practice in CaL-CO<sub>2</sub> capture plants to use another molar flow rate, called make-up flow rate, added in the calciner, substitung part of the recirculating solids (purge), as it can be seen in Fig. 2.1 in a CaL-CO<sub>2</sub> capture case. This make-up flow rate is composed by fresh CaO precursor that helps to increase the performance of the carbonator.

## 2.2 CaO carbonation behavior in the Ca-Loop

Of course, in a Ca-looping, the CaO grains have the main role. It is important to understand what happens to the grains, in the two reactors, when calcination or carbonation take place.

The operating conditions of the carbonator and of the calciner, as well as the grains dimensions, are important and may modify the reactions behavior between CaO and CO<sub>2</sub>.

The themogravimetric experimental study carried out by Benitez-Guerrero et al., in [7], analyzed the different behavior of the carbonation and calcination degree if they are under TCES or CO<sub>2</sub> capture operating conditions. In this work only the carbonation stage will be highlighted, since the final goal is to model a carbonator reactor.

As it can be seen from Fig. 2.4, there are differences in the carbonation behavior between the two different applications. First of all, the carbonation reaction can be divided in a first fast stage, which occurs on the free surfaces of the CaO particles, and a second slower stage controlled by the diffusion of the CO<sub>2</sub> in the CaCO<sub>3</sub> layer formed.

In TCES operating conditions, it can be seen how, the main contribution to CO<sub>2</sub> capture is given by the first fast stage, and this is because the concentration of CO<sub>2</sub> is higher than CCS applications, and it enhances the reaction kinetics. As a contrary the slow reaction stage contribution is almost negligible.

On the other hand, under CO<sub>2</sub> capture operating conditions is the opposite, the fast reaction stage is hindered due to the low CO<sub>2</sub> partial pressure typical of this technology, but the slow diffusion stage is promoted under these conditions.

Another critical aspect in the calcium looping is the mineral used to carry out the process. The CaO precursors are widely abundant and cheap minerals, they can be dolomites or limestones minerals. The main difference that can be noticed using different CaO precursor is the carbonation level reached by the particles in the carbonator, the so called muticycle activity. Indeed, as it can be seen from Fig. 2.5, the maximum carbonation conversion achievable changes from a cycle to cycle, and different mineral precursors shows different deactivation. This is a phenomenon related to the sintering process that can happen in the calciner. Under operating conditions typical of TCES technology, the deactivation of the particles

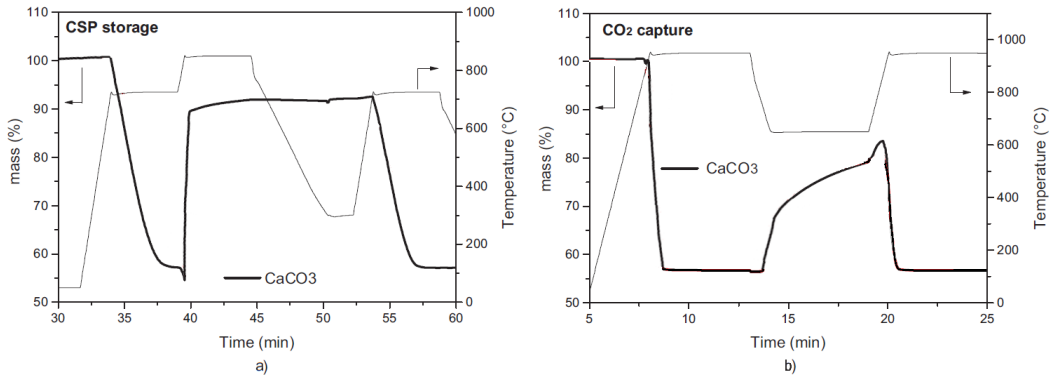


Figure 2.4: Thermogravimetric analysis for the first carbonation cycle, for particles with diameter smaller than  $45 \mu m$ , under TCES conditions (a) and CO<sub>2</sub> conditions (b) [7]

decreased much less than the deactivation curves under CCS conditions, for both the minerals.

The differences in deactivation, between the two technologies, are due to the harsh calcination conditions in CaL-CO<sub>2</sub> capture applications that lead to higher sintering of the CaO grains, and so to reduce the free surface needed for the reaction.

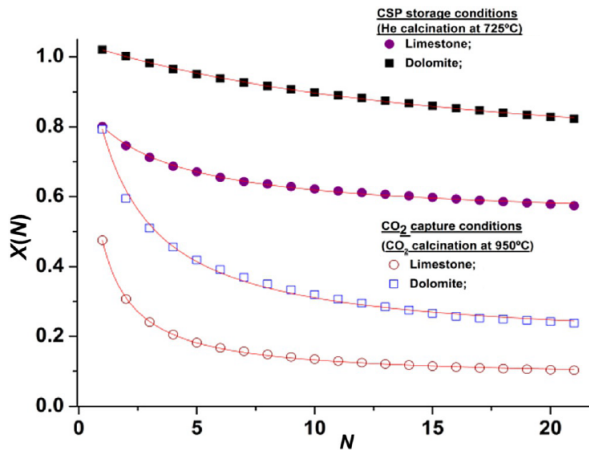


Figure 2.5: Multicycle activity of dolomite and limestone for CaL-CO<sub>2</sub> capture conditions and for CaL-CSP conditions for particle diameter smaller than  $45 \mu m$

On the other hand the lower deactivation behavior of the dolomite is explained by the presence of inert MgO grains segregated in the CaO structure. These grains, presumably, hinder aggregation and sintering of the CaO grains in the calciner, and so increase the efficiency of the Ca-Loop.

# Chapter 3

## Fluidized bed

As already said in Section 2.1, the circulating fluidized bed is the technology used for reactors in the ca-looping. Circulating fluidized bed belongs to the big category of the heterogeneous reactor, in which gas and solid, or liquid, react. The terms fluidization refers to the process by which the solid (particles) is transformed in a fluidlike state through suspension in a gas [4].

In this section the technology of the fluidized bed is introduced, from the fixed bed to the circulating fluidized bed reactor.

### 3.1 Gas-solid contacting regime

Depending on the gas velocity and the particle characteristics, the contacting regime between the two phases can be different.

Starting from low velocities, of the order of cm/s, the gas merely percolate through the voids between the particles that are fixed without appreciable motion, this is called fixed bed. If the velocity is slightly increased the particles start to vibrate, and this is called expanded bed.

When the drag force applied on the particles by the gas, becomes equal to the weight of the particles, the regime of the bed is considered at minimum fluidization. Here the height of the bed increases (see Fig. 3.1) and the particles become to behave like a liquid state suspended by the flowing gas. The velocity for which this

condition happens is called minimum fluidization velocity,  $u_{mf}$ , the voidage in the bed is  $\epsilon_{mf}$  and the height of the bed is  $L_{mf}$ .

When the gas velocity increases large instabilities in the particles vibrations give rise to formations of upwards gas bubbles and channels of gas. In this regime, as a first approximation, the excess of gas ( $u_0 - u_{mf}$ ) passes through the bubbles, which rises as in a liquid with low viscosity. The voidage of the bed, except the bubbles, remains at  $\epsilon_{mf}$  and it does not expand much more beyond  $L_{mf}$ . Depending on the grain size, the bubbles will move near the wall or in the middle of the bed, but in both the cases the solid mixing will be increased with respect to the fixed or minimum fluidized bed.

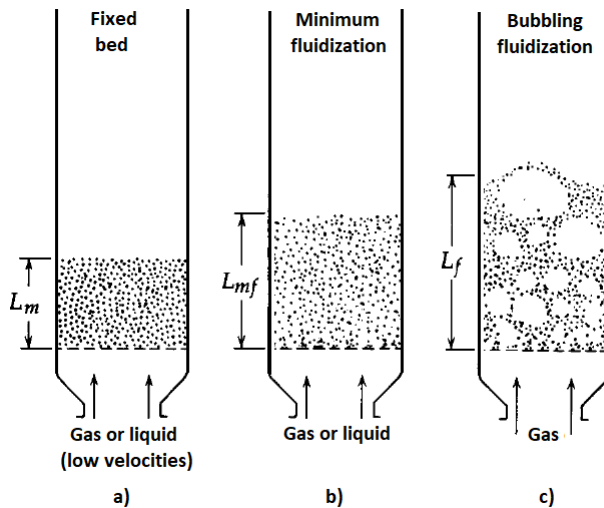


Figure 3.1: Contactig regimes [4]

If the velocity exceed the so called terminal velocity,  $u_t$ , characteristic of the particles geometry used, besides the increasing in bubbles, the particles which were ejected from the bed surface, due to the bursting bubbles process, starts to be entrained much higher in the riser till the maximum height of the reactor. This is called turbulent regime. Since there would be many particles which would leave the reactor, entrained by the high gas flow rate, they have to be collected by cyclone, that, in turbulent fluidized bed can be inner type cyclones, since the

entrainment is moderate (Fig 3.2).

If the velocity is so high that the inner cyclone does not allow a steady state working, it needs outer bigger cyclone, one or more, outside the reactor, and so a recirculating system (Fig. 3.2) composed by a downcomer that connects the cyclone to the loop seal, where the particles are collected, fluidized again and sent to the bottom of the reactor. This regime is called "fast fluidization regime", it guarantees the highest mixing and it is mostly used in application where a large volumetric flow rate must be treated.

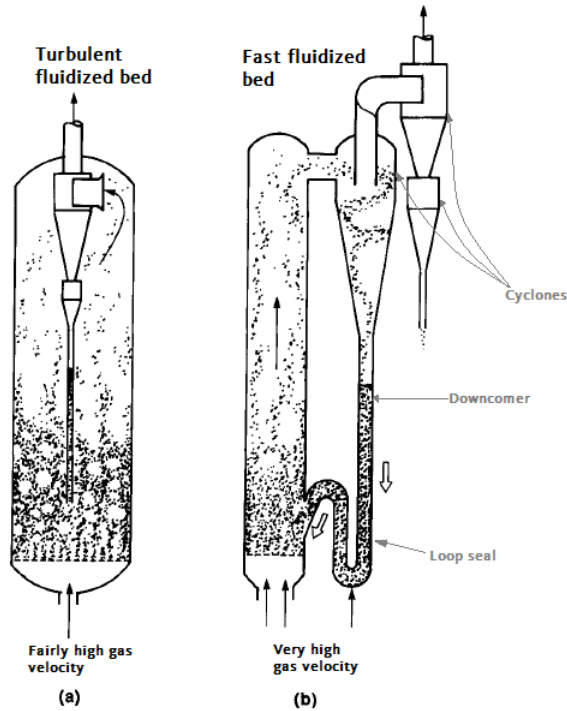


Figure 3.2: Turbulent fluidized bed (a), fast fluidized bed (b) [4]

### 3.1.1 Cyclone

Since with high gas velocity the particles can exit the reactor to separate gas and solid phase, in order to introduce again the particles in the reactor, a cyclone is

used. A cyclone is a device which separates the solids from a gas stream thanks to radial centrifugal force exerted on the particles. They have no moving part, and so they are cheap with low maintenance cost [31].

The efficiency of this devices is measured as a function of the particles residue exiting the cyclone with gas. Coarser particles will be separated easily by the cyclones.

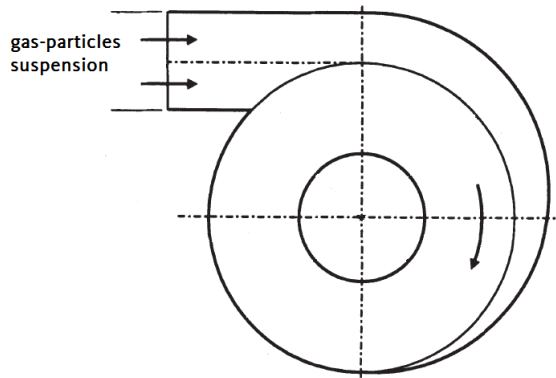


Figure 3.3: Cross sectional view of a cyclone [31]

### 3.1.2 Standpipe-loop seal

After the cyclone, particles fall down through a tube, called standpipe or downcomer. They can arrive to the loop seal, circulating again in the reactor, or they can exit the reactor going to the regenerator, thanks to a valve that can be installed in the downcomer.

The loop-seal transfers the solid from low pressure region of the outlet, to the high pressure region of the bottom part of the reactor. The loop seal is composed by two section [9]: a supply and a recycle section. The solids is collected in the supply section where it is fluidized using aeration nozzles. This flow proceeds to the recycle section and finally comes back to the reactor riser (this mass flow is called overflow). A schematic representation of the standpipe-loop seal is reported in Fig. 3.4.

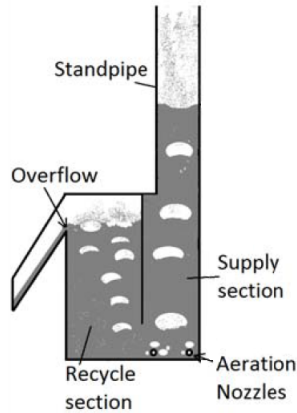


Figure 3.4: Standpipe-loop seal arrangement [9]

## 3.2 Geldart particles classification

Depending on their characteristics, powders can behave differently when fluidized by a gas. Geldart in [10] classified powders with respect to their behavior if fluidized. They are defined 4 categories of powders:

- Geldart A, when they are fluidized they exhibit a considerably bed expansion before the bubbling commences, bubbles appear to split and recombine very frequently increasing the mixing rate, they fluidize easily, and are called aeratable;
- Geldart B, the bed expansion is small, they fluidize well with vigorous bubbling action and large bubbles, are called sandlike, the most used in gas/solid reactors;
- Geldart C, their fluidization is difficult due to the high interparticle forces, called cohesive powders;
- Geldart D, difficult to fluidize, they behave in a unpredictable way, called sputable.

A classification diagram of the powder for fluidization is reported in Fig. 3.5, where the different classes are divided with respect to the mean particles diameter and the difference of density solid/gas.

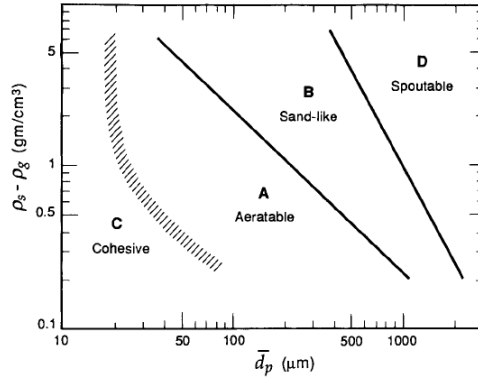


Figure 3.5: Classification of solids depending on their behavior when fluidized [4]

### 3.3 Mapping of fluidization regimes

To predict the behavior of the gas/solid contact, that will influence the performance of the reactor, it needs to know the working regime of the fluidized bed. Different investigators have collected experimental studies trying to find a relationship between particle characteristics, and operating conditions. The diagram most useful for engineering applications is the map regime diagram proposed by Grace in [11] (Fig 3.6), which relates the dimensionless particles diameter and the dimensionless velocity, defined as:

$$d_p^* = d_p \left[ \frac{\rho_g (\rho_s - \rho_g) g}{\mu^2} \right], \quad u^* = u \left[ \frac{\rho_g^2}{(\rho_s - \rho_g) g} \right]^{1/3} \quad (3.1)$$

Thus, once that this two dimensionless value are know, or are fixed, it is possible to know the probable gas/solid contact regime in which the reactor is working.

### 3.4 Circulating fluidized bed

As already said in Section 3.1, increasing the superficial gas velocity,  $u_0$ , the particles motion becomes more and more violent until, passing through a turbulent regime, it reaches the so called fast fluidization regime. In this regimes, thanks to the high volume flow rate used for fluidization, it is possible to use smaller

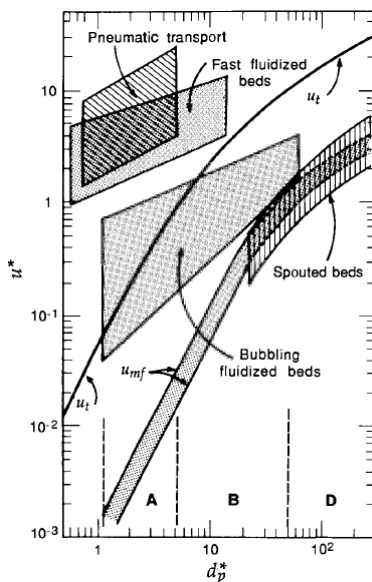


Figure 3.6: Map regime diagram of fluidized beds [11]

cross-section than BFB or TFB, and consequently they have lower costs.

The peculiar aspect of these working conditions is that there is no more a clear separation between the solid lower bed region of the reactor and the freeboard, as it was for the bubble or turbulent fluidized regime ([4]), but what is observed from the first time by Li and Kwauk in [12] is an evident S-shaped axial voidage profile, with a gradual transition from the dense region to the dilute region.

The laws that control the motions of the particles in a CFB are complex. Experimental studies carried out by Weinstein [17], Monceaux [18], and Hatrge [20], show the distribution of voidage and the local flux of solids in the cross section, and it's clear how solids favour the flowing upwards in the core zone, against the downward solids flowing observed near the wall.

On the one hand, for the reactor bottom region, denser in solid, the regime is very similar to the bubbling or turbulent regime. Here the mixing is the highest. The solid mass flow rate that comes from the upper dilute region is mixed with the solids arriving from the recirculation system and from the regenerator (from the calciner in the case of Ca-looping).

On the other, going upwards, the solids clumps that are thrown from the gas into the freeboard, begin to decrease in density, losing particles from the clumps to the near wall region, where they fall again in the bottom part. So higher is the height of the reactor, lower will be the density of the clumps that arrive at the exit, until the extreme condition, only in the tallest reactors, in which the clumps are completely dissolved in a dilute flow with only particles going upwards. A representation of this flow regime is reported in Fig. 3.7.

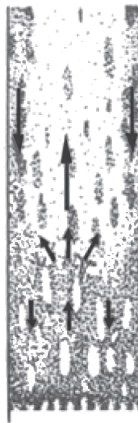


Figure 3.7: Sketch of a fast fluidized regime [31]

## Chapter 4

# Ideal models for chemical reactors

A chemical reactor is a limited volume where a chemical reaction takes place, to convert the reactants in the final products desired. The most common classification of the reactor is about the phases involved in the reactors, and so it is possible to divide them in *homogeneous reactors* and *heterogeneous reactors*.

Chemical reaction engineering has the aim of properly designing chemical reactors, using the knowledge from different areas of engineering: thermodynamics, fluid mechanics, chemical kinetics, mass transfer and heat transfer. To design correctly a reactor, means to predict the performance, what is happening or what it could happen in the reactor, through a series of mathematical relationship. The function that relates input to output is called performance equation and it can be composed by two main parts: the contacting pattern, how the materials flow through the reactor and contact each other, and the kinetics, namely how fast the things happen.

Ideal reactors models are easy ways to treat the chemical reactors, and in reality it is very often tried to make real reactors similar to the ideal ones. They are classified as:

- batch reactors;

- continuous-flow reactors, that can be: continuous stirred tank reactors (CSTR), plug flow reactors (PFR) or packed bed reactor (PBR).

In this section the ideal reactor models are introduced, highlighting the main design variables for each of them, in order to be more aware of their applications in the carbonator model that will be introduced later on.

## 4.1 Batch reactors

A batch reactor is an ideal reactor which works in transient conditions. During the reaction there are not inflows or outflows, and so applying the general mole balance for the general chemical component  $j$ :

$$F_{j,in} - F_{j,out} + r_j V = \frac{dN_j}{dt} \quad (4.1)$$

it becomes equal to:

$$\frac{dN_j}{dt} = \int^V r_j dV \quad (4.2)$$

The chemical composition is uniform everywhere in the reactors, but it changes with time. A representation of the mixing pattern that takes place in a batch reactor is reported in Fig. 4.1.

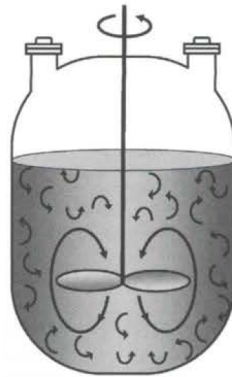


Figure 4.1: Representation of the contact regime in a batch reactor [15]

If the reaction  $A \rightarrow B$  is considered, the aim of the design process could be to know what time,  $t_1$ , is needed to reduce the species  $A$  from  $N_{A0}$  to  $N_{A1}$ , knowing the reaction rate  $r_A$ . So, starting from eqn. (4.2), assuming an uniform reaction rate in the reactor, it is possible to find the time needed as:

$$t_1 = \int_{N_{A0}}^{N_{A1}} \frac{dN_A}{r_A V} \quad (4.3)$$

## 4.2 Continuous flow reactor

A continuous flow reactor always operates in steady state conditions. They can be divided in:

- continuous-stirred tank reactors (CSTR);
- plug flow reactors (PFR);
- packed-bed reactors (PBR).

### 4.2.1 Continuous-stirred tank reactor (CSTR)

A CSTR, sometimes called mixed flow reactor, normally operates in steady-state conditions, and is assumed perfectly mixed, thus, there is no dependence of the temperature, concentration or reaction rate with respect to space or time. As a consequence, the concentration of the outflow will be the same as the reactor one. The general mole balance, equation (4.1), becomes:

$$F_{j0} - F_j = r_j V \quad (4.4)$$

So, knowing the reaction rate, with an imposed conversion  $X = (F_{j0} - F_j)/F_{j0}$ , it is possible to calculate the necessary volume as:

$$V = \frac{F_{j0} X}{-r_j} \quad (4.5)$$

A representation of the contacting pattern in a CSTR is reported in Fig. 6.14.

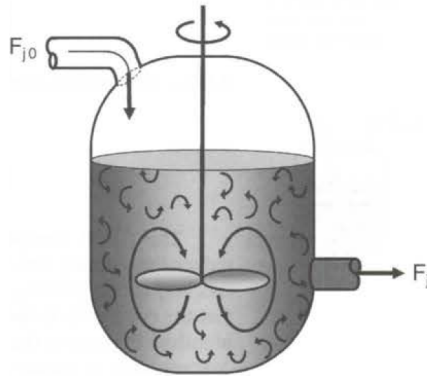


Figure 4.2: Representation of the contacting pattern in a CSTR [15]

## 4.2.2 Plug-flow reactor (PFR)

A plug-flow reactor is a particular case of what is called tubular reactor. This kind of ideal reactor is used for flow rate in turbulent conditions, where the axial diffusion of the chemical species is neglected, and gas velocity, temperature and concentration are assumed uniform in the cross section, so with a infinite radial diffusion.

In this case it needs to apply a mole balance to a finite volume, to understand how the molar flow rate changes in its travel.

Considering steady state conditions, and taking  $dV$  sufficiently small to consider the reaction rate uniform in this volume, the mole balance on the finite volume (represented in Fig. 4.3) can be written as:

$$F_j|_V - F_j|_{V+dV} + r_j \Delta V = 0 \quad (4.6)$$

Thus, taking the limit as  $\Delta V$  approaches zero, it is obtained the differential form which governs the molar flow rate evolution of a species in a PFR:

$$\frac{dF_j}{dV} = r_j \quad (4.7)$$

Expressing 4.7 as a function of conversion  $X$ , it is possible to calculate the

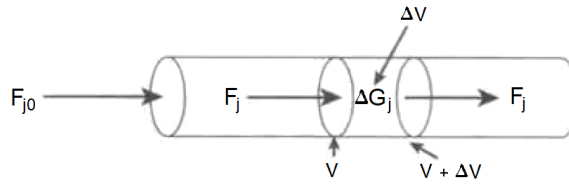


Figure 4.3: Mole balance applied to a finite volume for the species  $j$  in a PFR [15]

necessary reactor volume to achieve a certain conversion, knowing the reaction rate, with 4.8.

$$V = F_{j0} \int_0^X \frac{dX}{-r_j} \quad (4.8)$$

So, depending on the reaction rate, the reactor has to be larger or smaller to achieve the conversion desired. A typical form of the conversion rate is the first order dependence, if the reaction  $A \rightarrow B$  is considered:

$$-r_A = kC_A = kC_{A0}(1 - X) \quad (4.9)$$

and so:

$$\frac{1}{-r_A} \propto \frac{1}{X} \quad (4.10)$$

thus, using 4.10 in 4.8 it can be seen how if it is desired a reactor which totally converts the reactant  $A$ , it would be necessary a reactor of infinite volume, so sometimes it is impossible to reach the complete conversion desired using continuous flow reactors. The same is in equilibrium reactions, where the conversion approach asymptotically the equilibrium conversion  $X_e = \frac{C_{A,in} - C_{A,eq}}{C_{A,in}}$ , instead of  $X = 1$ .

### 4.2.3 Packed bed reactor (PBR)

Packed bed reactors are characterized by the reaction between solid and gas, that slowly percolates through a fixed bed of solid particles. In this reactor the reaction rate is based on the mass of the catalyst,  $W$ , instead of the reactor volume,  $V$ .

Using the same strategy of the PFR, the mole balance on a finite volume, reported in Fig. 6.14, characterized by a solid mass equal to  $\Delta W$ , can be written

as eqn. 6.14, for the generic species j.

$$F_j|_W - F_j|_{W+\Delta W} + r'_j \Delta W = 0 \quad (4.11)$$

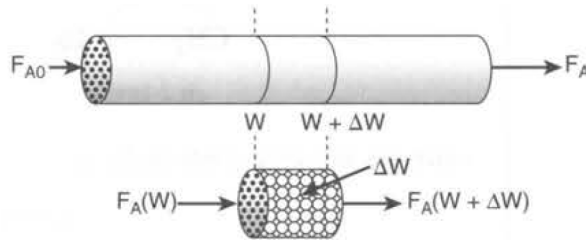


Figure 4.4: Scheme of a PBR

where  $r'_j$  is the number of moles that have reacted per unite of time, per unit of solid mass ( $mol/(s \cdot kg)$ ) So, taking the limit as  $\Delta W$  approaches zero, the differential form useful to calculate the variation in molar flow rate of the species is:

$$\frac{dF_j}{dW} = r'_j \quad (4.12)$$

In this case the design variable is not the reactor volume, but the weight of the solid, and so if the reaction rate is known, and it is required a conversion of j from  $F_{j0}$  to  $F_j$ , the mass of solid needed is:

$$W = \int_{F_{j0}}^{F_j} \frac{dF_j}{r_j} \quad (4.13)$$

## Chapter 5

# Carbonator numerical model

Coming back again to the fluidized bed and to the particular application desired, when the gas velocity is increased, the drag force applied on the particles can become so high that the grains can exit from the reactor. In these regimes a solid recirculating system is needed in order to keep a constant solid inventory. These are the Circulating Fluidized Bed, or also called fast fluidized bed, and nowadays are used especially as Fast Catalytic Cracking reactors or combustors. In the ca-looping the regime suggested for the carbonator is the fast fluidized regimes, thanks to the high volume flow rate that it can reach with relatively small diameter.

In this section the carbonator numerical model used will be introduced starting from the developed concepts for CaL-CO<sub>2</sub> capture technology and, after that, focusing on the particular application CaL-CSP.

The carbonator model can be divided in three sub-models, as reported in Fig. 5.1. Having as input the operating conditions and the design variables, the hydrodynamic model aims to find the contacting pattern gas/solid, whose output are used for the chemical model, which gives the capture efficiency of the sorbent and so the energy released from the reaction. When the energy released is known is finally possible to compute the bed temperature and the power removed from the reactor using the energy model.

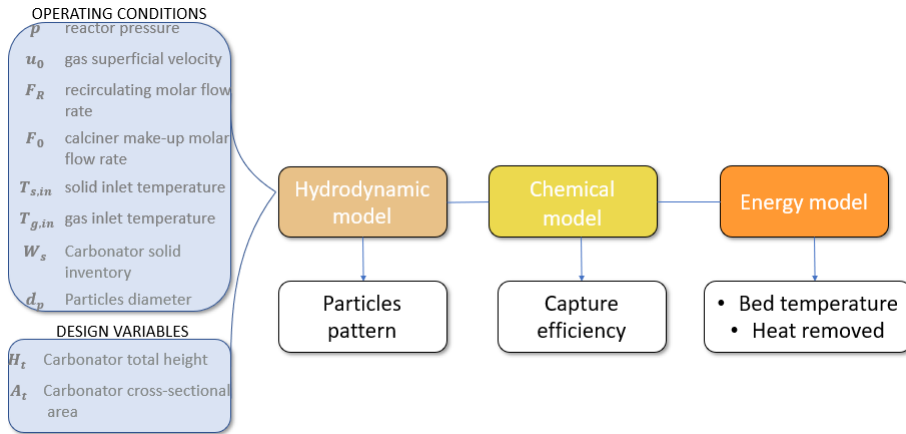


Figure 5.1: Concept diagram of the carbonator model

## 5.1 Hydrodynamic model

How the particles move in the reactor is a complex problem and different models are presented in the literature in order to try and solve analytically the movement of solid. Moreover, since the chemical reactions that occur are strictly related to the pattern of solids, and, in turn, the heat transfer, the hydrodynamic model is fundamental for a good design. Many papers in the literature focus on this problem, and generally the different kind of hydrodynamic models can be divided into three categories, as also defined by Pugsley et al. in [16]:

1. those models that predict only the axial variation of the solid volumetric fraction;
2. those models that predict both radial and axial variation of the solid volumetric fraction in the reactor;
3. those models based on the basic fundamental equations of fluid-dynamic.

### 5.1.1 Kunii and Levenspiel model

One of the most used hydrodynamic model, for bubbling fluidized bed before, and for fast circulating fluidized bed later, is the one proposed by Kunii and Levenspiel,

published in 1991 [4] for the first time, and then developed during the years in 1997 [21] and 2000 [22].

The K-L model is essentially based on experimentally observations, through which it has been possible to identify the key parameters that are useful to predict the 1D solid volumetric fraction in the reactor. They divided the riser in two regions: a denser bottom region, in which there is the highest cross sectional averaged solid volumetric fraction, and a lean region above, in which the solid volumetric fraction decreases with the height as eqn. (5.1),

$$f_l = f^* + (f_d - f^*) \exp(-az_l) \quad (5.1)$$

where,  $z_l$  is the height with respect to the height of the dense bed ( $H_d$ ) as also reported in Fig. 5.2,  $f_d$  is the cross sectional averaged solid volumetric fraction in the dense region, assumed constant throughout the region,  $f^*$  is the limit value that  $f_l$  can achieve, and  $a$  is the decay constant, an experimental parameter that describes the decreasing in solid density through the freeboard, and it is related to the exchange of particles from the upflowing clumps to the downflowing clumps placed near the wall. A sketch of the solid pattern and the solid density profile are reported in Fig. 5.2.

So, in order to use the model proposed by Kunii and Levenspiel, the values of  $f_d$ ,  $f^*$  and  $a$  have to be set. The best estimates for the value of  $a$  state that:

$$au_0 \cong \text{const}$$

for a certain Geldart class, and a value for each Geldart class is proposed. The values of  $f^*$  proposed are

- $f^* \leq 0.01$  for Geldart A solids
- $f^* \leq 0.02$  for Geldart B solids

About the value of  $f_d$ , it depends on the flow regime, in particular, for fast fluidized regime it is in the range  $0.06 \sim 0.22$ .

In this work it has been set  $f_d = 0.15$ ,  $f^* = 0.01$ , and  $a \cdot u_0 = 3 \text{ s}^{-1}$ , as also suggested by Romano in [24].

Besides the gas velocity, imposed from the inlet of the reactor, the throughflow

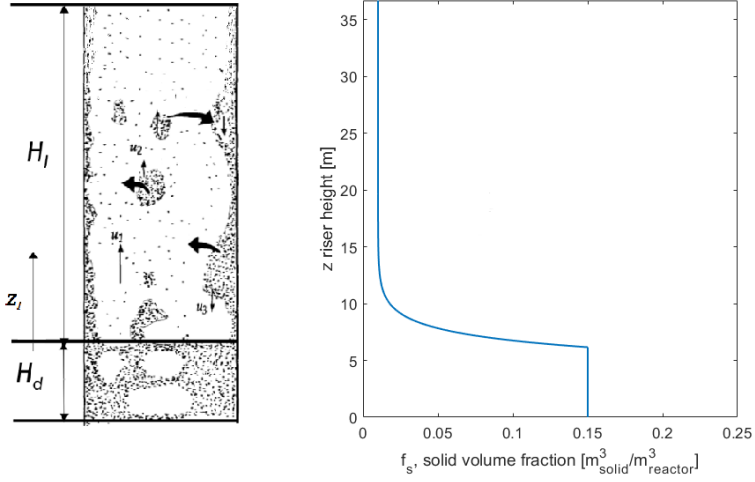


Figure 5.2: Sketch of the pattern in a fast fluidized regime reactor, on the left [21], and the exponential decay model of the solid volumetric fraction, on the right

of solids,  $G_s$ , and the solid inventory,  $W_s$ , are two other important variables when the design of a reactor is performed. About the solid inventory, it is possible to write a relationship between  $W_s$  and solid volumetric fraction in the dense and in the lean region, as reported in eqn. (5.2) [21]:

$$W_s = W_d + W_l = A_t \rho_s H_d f_d + A_t \rho_s H_l \bar{f}_l \quad (5.2)$$

where  $A_t$  is the reactor cross sectional area,  $\rho_s$  is the solid density,  $H_d$  is the dense region height,  $H_l$  is the lean region height ( $H_t - H_d$ ) and  $\bar{f}_l$  is the mean solid volumetric fraction in the lean region equal to:

$$\bar{f}_l = f^* + \frac{f_d - f_{se}}{aH_l} \quad (5.3)$$

where  $f_{se}$  is the exiting solid fraction.

About the throughflow of solids,  $G_s$ , it is the net solid flow that flows in the reactor and in the recirculation system, so it is constant along the height and in

general can be expressed as [4]:

$$G_s = \rho_s f_s u_s \quad (5.4)$$

where  $u_s$  is the mean solid velocity of the solid. Knowing that  $u_s = u_g - u_p$ , where  $u_p$  is the gas/solid slip velocity, the exit mass flow rate per unit cross section will be (5.5).

$$G_{se} = \rho_s f_{se} \left( \frac{u_0}{1 - f_{se}} - u_p \right) \quad (5.5)$$

With the assumption of  $f_{se} \ll 1$  (particles dispersed in the gas flow) and  $u_p \cong u_t$ , valid in the case of completely dispersed particles, it is possible to write (5.6).

$$G_s = G_{se} \cong \rho_s f_{se} (u_0 - u_s) \quad (5.6)$$

The main output from the hydrodynamic model is the dense region height, that can be found with the system of equations composed by eqns. (5.1), (5.2), (5.3) and (5.6) in two different ways: with fixed solid inventory,  $W_s$ , or with a fixed net solid flow,  $G_s$ . In the model introduced a solid inventory in the reactor is fixed, and so with imposed values of  $a$ ,  $f_d$  and  $f^*$ , using eqns. (5.2) and (5.3), and knowing that  $H_d + H_l = H_t$ , it is possible to find the value of the dense region height,  $H_d$ , and so the solid volumetric fraction in the outlet of the reactor,  $f_{se}$  and the entrainment flow  $G_s$ .

### 5.1.2 Core/annulus model

It exists also a distribution of solids in the radial direction of the reactor. As already said in Section 5.1.1, the particles move upward in the core region, and downward in the region near the wall.

To model this finding most of the authors have adopted the so called core/annulus model dividing the cross section in two regions: a central core region, with few particles dispersed in the gas flow, and a wall region rich in solids. The same value of  $f$  is assumed for the wall zone in the dense and lean region, as well as the value of  $f$  for the core zone in the dense and lean region, as suggested in [21]. So

it can be written that:

$$f_{dw} = f_{lw} = f_w \quad (5.7)$$

$$f_{dc} = f_{lc} = f^* \quad (5.8)$$

where  $f_w$  is set equal to 0.5.

With these assumptions, applying a material balance at any level of the carbonator, it is possible to find the ratio between the core region volume and the volume of the reactor, in the dense and lean regions,  $\delta_d$  and  $\delta_l$  respectively, as written in (5.9) and (5.10).

$$\delta_d = \frac{f_w - f_d}{f_w - f^*} \quad (5.9)$$

$$\delta_l(z) = \frac{f_w - f_l(z)}{f_w - f^*} \quad (5.10)$$

This core/annulus structure understanding will be important when the gas phase is modelled, since how the particles are distributed in the cross section could modify the reaction rate, in particular if there are areas of the reactor that are difficult to reach by the gas flow due to the high density of particles.

The situation modelled, using these assumptions, is shown in the sketch of Fig. 5.3.

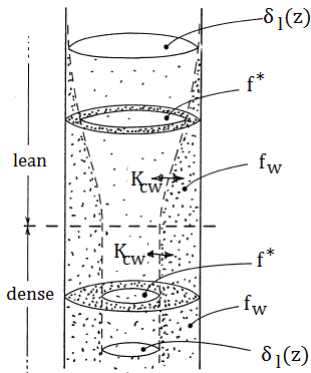


Figure 5.3: Sketch of the core/annulus model used [22]

## 5.2 CaO carbon capture capacity

In a Ca-looping, the carbonator is the component of the plant where the exothermic reaction between the  $\text{CO}_2$  and  $\text{CaO}$  takes place. After that this two reactants have reacted, the  $\text{CaCO}_3$  formed is sent to the calciner to start again a new cycle.

Studies in literature proved that the carbonation of the calcium oxide is far from the reversibility.

First of all, as already said in Section 2.2, the reaction can be split in two stages, a fast reaction stage on the surface and a slow diffusion controlled reaction stage. But, when the particles is calcined and carbonated, so when it passes from the carbonator to the calciner again in the carbonator, the kinetically controlled stage will be shorter, and so it will experience lower carbonated fraction in the same permanence time in the reactor than when it was at the first carbonation. [25]

Grasa et al. in [25] measured experimentally the variation of the particles weight as a function of time, simulating typical  $\text{CO}_2$  capture cycles and, using this data, they extrapolated the variation of the carbonation degree in which the reaction becomes dominated by the diffusion of  $\text{CO}_2$ , also called maximum value of carbonation,  $X_{max,N}$ , since the reaction rate in the diffusion stage is usually almost zero. The results of the TGA are reported in Fig. 5.4, and equation (5.11) is the experimental relationship extrapolated.

$$X_{max,N} = \frac{1}{\frac{1}{1-X_r} + k_{deact}N} + X_r \quad (5.11)$$

In equation (5.11),  $X_r$  and  $k_{deact}$  are two parameters that fit the equation with the experimental data, called residual conversion and deactivation constant respectively, and in a typical  $\text{CO}_2$  capture application, with limestone as  $\text{CaO}$  precursor, are equal to  $X_r = 0.075$ , and  $k_{deact} = 0.52$ , whereas for carbonation at  $850^\circ\text{C}$  and calcination in He at  $725^\circ\text{C}$ , representative of CaL-CSP conditions,  $X_r$  is equal to 0.53 [19].

But there is also another aspect to take into account. In a continuous system, there could be particles that are cycled  $N$  times and others that are cycled  $N-20$  times or  $N+30$  times, since the time that a particle spend in the reactors is a

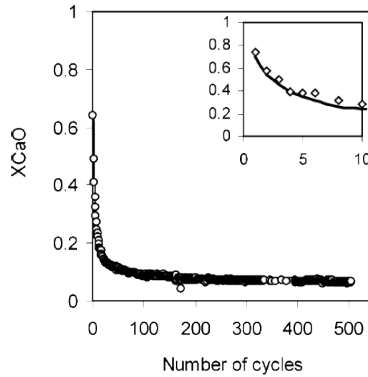


Figure 5.4: Sorbent conversion vs number of cycles for a typical CO<sub>2</sub> capture application

probabilistic matter. Thus, there is a wide range of particles with different cycles numbers, present in the system. If the system of Fig. 5.5 is considered, Abanades et al. in [26] carried out a mass balance to calculate the fraction of particles at the Nth cycle, reported here in eqn. (5.12), where  $F_0$  is the make-up flow of fresh limestone added in the calciner,  $F_R$  is the recirculating mass flow rate carbonator/calciner, and  $N$  is the number of the cycle.

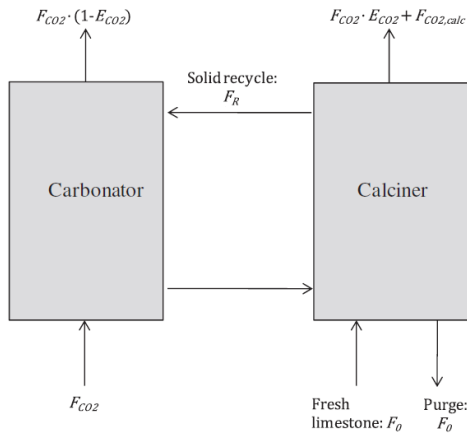


Figure 5.5: Schematic representation of the calcium looping system [24] in a CaL-CO<sub>2</sub> capture plant

$$r_N = \frac{F_0 F_R^{N-1}}{(F_0 + F_R)^N} \quad (5.12)$$

If the system experiences full carbonation and calcination, the maximum average activity of the particles in the reactor can be calculated as (5.13).

$$X_{max,ave} = \sum_{N=1}^{N=\infty} r_N X_{max,N} \quad (5.13)$$

It has to be noted that if the make-up flow is equal to 0, the average maximum carbonation will be equal to the residual conversion,  $X_{max,ave} = X_r$ .

### 5.2.1 Partial carbonation/calcination

What is assumed by Grasa et al. in [25] is the complete carbonation of the particles, so, they will reach the maximum carbonation, and the maximum calcination, in all the cycles. This is not always true under many configurations or operating conditions.

Grasa et al. in [27], studied the evolution of the maximum carrying capacity during the cycles, implementing the effect due to partial carbonation or calcination. It is proved that, if a particle of CaO experiences partial carbonation, after the calcination this particle is able to absorb more CO<sub>2</sub>, with respect to a particle that experienced full carbonation. In order to compare the performances of full carbonated particles, and partial carbonated particle, instead of using N, as the passages between one reactor and the other, it has defined  $N_{age}$  as the equivalent number of full carbonation/calcination cycles that a partial carbonated particles has to perform in order to have the same value of maximum carrying capacity,  $X_{max,N}$ . The results found in [27] are reported in Fig. 5.6, where Y, on the y-axis, is the number of moles of CO<sub>2</sub> absorbed per mole of CaO.

So, with partial carbonation/calcination conversions, the particles will be like younger particles than the ones which are experienced N full carbonation/calcination cycles (passage between the reactors). It is possible to define a cycle number

based on the level of consumption that they have experienced during partial carbonation/calcination and this will represent a reaction age, (eqn. (5.14)).

$$N_{age} = \frac{1}{k_{deact}} \left( \frac{1}{X_{ave} - X_r} - \frac{1}{1 - X_r} \right) \quad (5.14)$$

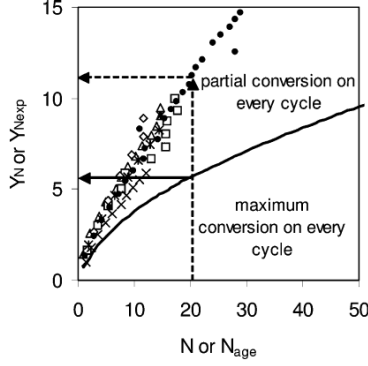


Figure 5.6: Moles of CO<sub>2</sub> transported with partial conversion or with maximum carbonation/calcination conversion as a function of N [27]

To take into account this phenomenon of decelerated aging, the fraction of calcination/carbonation in the calciner/carbonator are defined by eqns (5.15) and (5.16), and a mass balance, in each cycles, is carried out by Rodriguez et al., in [28], founding the final equation that represents the fraction of CaO particles that have experienced  $N_{age}$  equivalent carbonation cycles (5.17)

$$f_{carb} = \frac{X_{carb} - X_{calc}}{X_{max,ave} - X_{calc}} \quad (5.15)$$

$$f_{calc} = \frac{X_{carb} - X_{calc}}{X_{carb}} \quad (5.16)$$

$$r_{N,age} = \frac{\left[ \frac{F_0(1-f_{calc})}{F_0+F_R f_{calc}} + \frac{F_0}{F_R} \right] f_{carb}^{N_{age}-1} f_{calc}^{N_{age}}}{\left( \frac{F_0}{F_R} + f_{carb} f_{calc} \right)^{N_{age}}} \quad (5.17)$$

where  $X_{carb}$  and  $X_{calc}$  are the conversions of the solids that leave the carbonator and the calciner respectively. In the calciner, it is not difficult to reach a full calcination,

and so, also in this work a complete calcination,  $f_{calc} = 1$ , is considered, even because modelling the calciner is not the aim imposed.

Once  $r_{N,age}$  is defined, it is possible to calculate the value of maximum average conversion, with partial carbonation/calcination:

$$X_{max,ave} = \sum_{N_{age}=1}^{\infty} r_{N,age} X_{max,N} \quad (5.18)$$

As it can be seen from Fig. 5.7, if the partial carbonation increases the fraction of particles that can be found in the first stages of deactivation, with higher carrying capacity, is higher than when  $f_{carb}$  is equal to 1, and this is because they passed many times between the two reactors, and so they spend more time to arrive at the same degradation level of a particle which has experienced full carbonation, so, there will be more particles with higher carbonation capacity.

If, from the one hand, this phenomenon could seem advantageous because the particles have higher carrying capacity when  $f_{carb}$  is smaller, from the other hand, it has to be noted that, to increase the partial carbonation (or to reduce  $f_{carb}$ ), the recirculating mass flow rate ( $F_R$ ) has to increase much more, and this would cost a lot from the energy point of view, so, it is not obvious to say that the highest partial carbonation level is the best for the working of the plant.

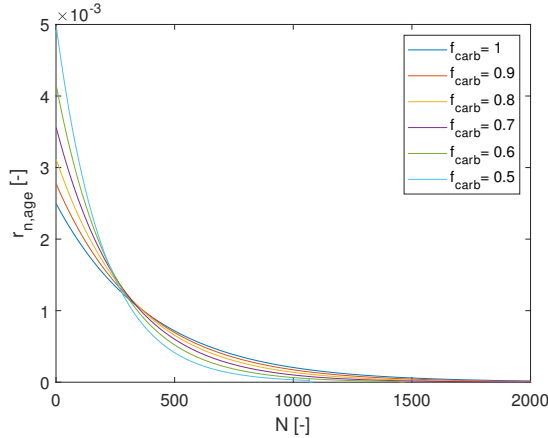


Figure 5.7: Fraction of CaO in the cycle  $N$ , or  $N_{age}$ , for different partial carbonation levels

### 5.2.2 Particles residence time

Besides the cycle number, the particles are characterized by a residence time in the reactor, which is a probabilistic quantity. To describes this probability, it is assumed that the particles are perfectly mixed in the reactor, which is justified by the high solid mixing and the high circulation rate of solids. The probability density function can be written as (5.19):

$$f_t = \frac{1}{\tau} \exp -(t/\tau) \quad (5.19)$$

where  $\tau$  is the average residence time defined as the fraction of moles of active particles,  $n_{s,a}$  (CaO and CaCO<sub>3</sub> in the carbonator), over the recirculation rate  $F_R$  (eqn. (5.20)).

$$\tau = \frac{n_{s,a}}{F_R} \quad (5.20)$$

So, if the recirculation rate decreases, or the solid inventory increases, the average residence time increases, as it was expected. If the particles pass through the reactor in short times, they could not have the time to react and absorb the CO<sub>2</sub>, and as a consequence the partiles partial carbonation will increase. So, even the average residence time is crucial for a good design.

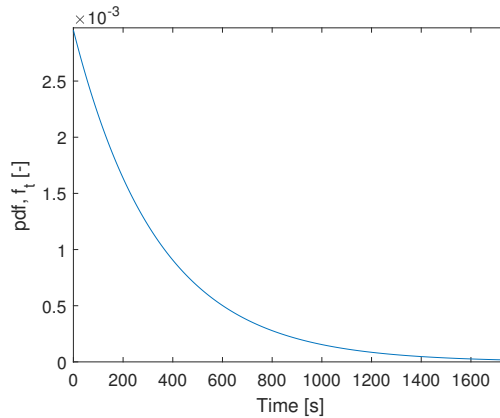


Figure 5.8: Typical profile of the pdf of the particles residence time

### 5.3 Gas kinetic model

During the permanence in the reactor, the  $\text{CO}_2$  in the flue gasses (in case of carbon capture plant), or the  $\text{CO}_2$  of the gas stream (in case of TCES plant), reacts with the  $\text{CaO}$ . To calculate the concentration of  $\text{CO}_2$  exiting the reactor, and so the capture efficiency of the carbonator, the reaction kinetic has to be studied.

The reaction between  $\text{CO}_2$  and  $\text{CaO}$  is a theoretical reversible first order reaction, driven by the difference of the working  $\text{CO}_2$  concentration and its concentration at equilibrium, that can be calculated as a function of the gas temperature using eqn. (5.21) [29] whose behavior is reported in Fig. 5.9, and the equation of state (5.22).

$$p_{\text{CO}_2,eq} = 4.137 \cdot 10^{12} \exp\left(\frac{-20474}{T}\right) \quad (5.21)$$

$$C_{\text{CO}_2,eq} = \frac{p_{\text{CO}_2,eq}}{R \cdot T} \quad (5.22)$$

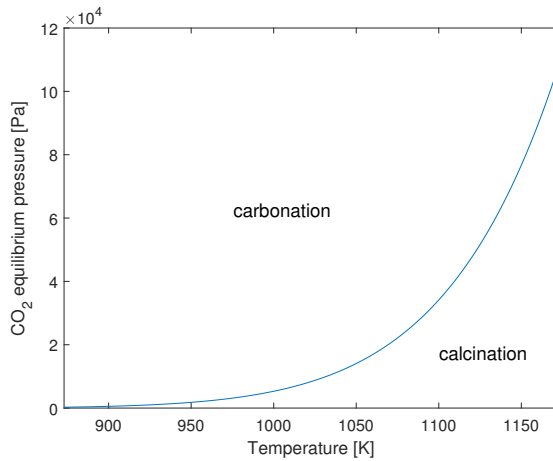


Figure 5.9: Equilibrium  $\text{CO}_2$  pressure based on eqn. (5.21)

Thus, the kinetic equation for the reaction



can be written as a first-order catalytic reaction using a plug flow model, eqn. 5.24, in which the concentration changes only in the longitudinal direction being uniform in the cross section, and the gas diffusion phenomenon, in the longitudinal direction, is considered negligible.

$$\frac{d(u_0(C_{CO_2} - C_{CO_2,eq}))}{dz} = -f \cdot k(C_{CO_2} - C_{CO_2,eq}) \quad (5.24)$$

in which  $k$  is the reaction rate constant expressed in  $s^{-1}$ . This variable is strictly related with the solid carbonation conditions in the reactor, and, to calculate the exact value of  $k$ , a solid phase kinetic model has to be used. This will be done later on in this Section.

Provided the value of  $k$ , the plug flow model introduced should be improved to describe the real situation of contact gas/particles.

As already seen in Section 5.1.2 the particles in the reactor are distributed in two regions: core and wall region. In these two regions the carbon dioxide can interact and react with them, quickly or slowly depending on the reaction rate constant,  $k$ . As assumed by Kunii and Levenspiel [21],[22], the gas velocity in the wall region is assumed negligible, it means that the gas flow rate passes almost entirely through the core region, but, due to gas diffusion, there are still some reactions near the wall. To model this phenomenon, a contact efficiency is introduced, which takes into account the difference existing between the real flow, in which the gas velocity in the wall region is assumed negligible, and an ideal plug flow, where the gas velocity is uniform everywhere. Thus, 5.24 is re-written as:

$$\frac{d(u_0(C_{CO_2} - C_{CO_2,eq}))}{dz} = -f \cdot \eta_{plugflow} \cdot k(C_{CO_2} - C_{CO_2,eq}) \quad (5.25)$$

About the dense lower region, the contact efficiency,  $\eta_d$ , can be written as:

$$\eta_d = \frac{[f_{limit} \cdot \delta_d + \frac{1}{1/(\delta_d \cdot k_{cw}) + 1/(f_w(1-\delta_d))}]}{f_d} \quad (5.26)$$

and for the lean upper region, it is used an increasing exponential behavior, characterized by the experimental coefficient,  $b = 6.62m^{-1}$  [4]:

$$\eta_i = 1 - (1 - \eta_d)e^{-b \cdot z_i} \quad (5.27)$$

For a better understanding of the possible reaction ways, it can be also thought an equivalent circuit, from the reactants to the products, reported in Fig 5.10, for the dense region case.

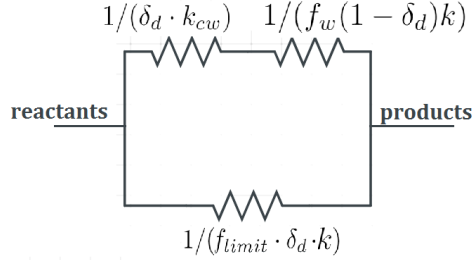


Figure 5.10: Equivalent electrical circuit of the carbon dioxide reaction, to go from the reactants to the products

It has to be noticed that if the parameter  $k_{cw}$  goes to infinite, and so there is not resistance to the diffusion of the gas in the cross section, the plug flow efficiency goes to 1, that is the case of an ideal plug flow.

With the eqns. 5.25, 5.26 and 5.27, and assuming a constant superficial velocity in the reactor, the relationship between inlet  $CO_2$  concentration,  $C_{CO_2,in}$ , the  $CO_2$  concentration just above the dense region,  $C_{CO_2,d}$ , and the outlet concentration,  $C_{CO_2,ex}$ , are written as:

$$\ln \frac{(C_{CO_2,in} - C_{CO_2,eq})}{(C_{CO_2,d} - C_{CO_2,eq})} = \frac{k \cdot H_d}{u_0} \left[ 1/f^* \cdot \delta_d \cdot k + \frac{1}{1/(\delta_d \cdot k_{cw}) + 1/(f_w(1 - \delta_d)k)} \right] \quad (5.28)$$

$$\ln \frac{(C_{CO_2,d} - C_{CO_2,eq})}{(C_{CO_2,ex} - C_{CO_2,eq})} = \frac{k \cdot f^*}{u_0} \left[ H_l - \frac{1 - \eta_d}{b} (1 - e^{-bH_l}) \right] + \frac{k(f_d - f_{limit})}{u_0} \left[ \frac{1 - e^{-aH_l}}{a} - \frac{1 - \eta_d}{a + b} (1 - e^{-(a+b)H_l}) \right] \quad (5.29)$$

What is still missed is the reaction rate constant,  $k(s^{-1})$ .

## 5.4 Solid kinetic model

The reaction kinetic of the gas phase is strictly related to the carbonation degree that the solid has reached. This is not a constant value for all the particles in the reactor, it changes during the permanence time, from the inlet to the outlet, but also, in steady state conditions, there will be different particles that have experienced different times the calcination reaction, and so, their maximum carbonation degree achievable ( $X_{max,N}$ ) is different (eqn.5.11).

All these observations bring to the requirement to model the particles as perfectly mixed in the reactor, assumption also supported by the high mixing that a fast fluidization regime involves. In an ideal perfectly mixed reactor the concentration of the chemical species are uniform in the whole reactor, and so the exiting concentration of an element is exactly the same as the reactor one (as explained in Section 4.2.1).

Using the probability density function 5.19 that describes the residence time probability of a particle in the reactor, it is possible to know how many particles have reacted for that certain time, but what we still don't know is the carbonation that they have reached in this permanence time. A reaction rate equation for the solid is needed.

Various reaction models have been proposed in literature, based on particles structural properties, and a possible general classification, defined by Martínez et al. in [3], divides them in:

- grain models, which use the classical grain model expression from Nitsch

(1962), and represent the particle as a porous structure

- and pore models, which consider the evolution of the pore size distribution during the carbonation.

The model adopted in this work, belongs to the family of those models developed by different authors that use the grain model fundamental equation, including parameters defined in the pore model. It is proposed by Grasa et al. in [30], used later by Romano [24], and useful to calculate the particles carbonation behavior in time. According to [30] the carbonation rate can be expressed as eqn. (5.30)

$$\begin{aligned} \frac{dX_{carb}}{dt} &= k_r(C_{CO_2} - C_{CO_2,eq}) \\ &= k_s S_N (1 - X_{carb})^{2/3} (C_{CO_2} - C_{CO_2,eq}) \end{aligned} \quad (5.30)$$

where  $k_s$  is the intrinsic reaction rate constant, found to be  $6.05 \cdot 10^{-10} m^4/mol/s$  and basically independent by the temperature [30].  $S_N$  is the surface area available for the reaction on a particle after N calcinations, it changes with N and it is assumed equal to:

$$S_N = \frac{V_{M,CaCO_3} X_{max,N}}{M_{CaO} h} \rho_{CaO} \quad (5.31)$$

where  $h$  is the product layer that is formed on the reaction surface,  $S_N$ , at the end of the fast reaction stage, and is almost constant in different cycles [5], it is equal to 50 nm in CaL-CO<sub>2</sub> capture conditions and to 100 nm in CaL-CSP capture conditions [7].

Different authors in literature calculate the capture efficiency of the reactor using also the second diffusion phase reaction (Ortiz et al. [8]), but most of them consider the rate of reaction after the end of the fast reaction stage equal to zero. This assumption is valid, in particular, in case of high concentration of carbon dioxide, as in the case of TCES application, where the gas stream is only composed by CO<sub>2</sub>. Here the same carbonation behavior obtained by Romano [24] is used. In particular, when the permanence time of the particle is lower than the time needed to reach the end of the fast reaction stage,  $t_{lim}$ , expressed with eqn. 5.33,  $X_{carb}(t)$

is obtained from the integration of (5.30), whereas when the permanence time is higher than  $t_{lim}$ , the reaction rate constant is assumed equal to 0 for  $t > t_{lim}$ , and so the carbonation level of the solid is kept constant in time. This is reported in eqn. (5.32).

$$X_{carb}(t) = \begin{cases} 1 - [1 - \frac{k_s S_N (C_{CO_2} - C_{CO_2,eq})}{3} t] & \text{if } t < t_{lim} \\ X_{max,N} & \text{if } t > t_{lim} \end{cases} \quad (5.32)$$

$$t_{lim} = \frac{k_s S_N (C_{CO_2} - C_{CO_2,eq})}{3[1 - (1 - X_{max,N})^{1/3}]} \quad (5.33)$$

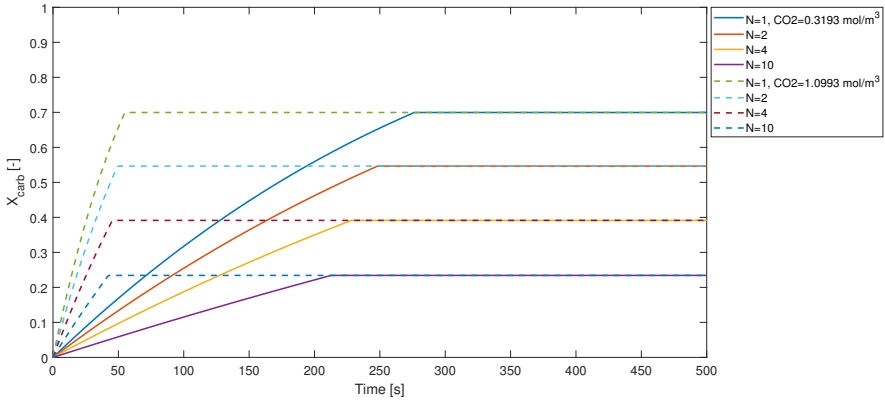


Figure 5.11: Carbonated particles fraction as a function of time parameterized for different carbonation cycles and equivalent  $CO_2$  concentration at which it is exposed

As it can be seen from Fig. 5.11, if the  $CO_2$  concentration increases, the reaction will be faster, or, if the number of time the particle has been cycled moves on, the maximum carbonation decreases, as well as the reaction rate.

Once that the carbonation degree behavior is known, with eqns. (5.19) and (5.17), the total average carbonation degree of the particles in the reactor can be

evaluated as ([24]):

$$\begin{aligned}
 X_{ave} &= \sum_{N_{age}=1}^{\infty} r_{N,age} \int_0^{\infty} f_t X_{carb}(t) dt \\
 &= \sum_{N_{age}=1}^{\infty} r_{N,age} \left( \int_0^{t_{lim}} f_t X_{carb}(t) dt + \int_{t_{lim}}^{\infty} f_t X_{max,N} dt \right)
 \end{aligned} \tag{5.34}$$

This is the most important equation in the solid reaction model. It takes into account most of the concept introduced in this section: the distribution with respect to the number of cycles experienced and the effect of partial carbonation ( $r_{N,age}$ ), the residence time probability in the reactor,  $f_t$ , and the carbonation time behavior,  $X(t)$ , which is influenced by the gas concentration in the reactor and the number of complete calcination performed, as it can be seen from Fig. 5.11.

Once that the kinetic of calcium oxide as CO<sub>2</sub> sorbent is defined, it is possible to calculate the first order kinetic constant,  $k$ , in terms of  $s^{-1}$ , in order to use the K-L model and the gas kinetic model, introduced in Section 5.3 . Using eqn. 5.30, and knowing that  $k = k_r \frac{\rho_{s,a}}{M_{s,a}}$ , and with the eqns. 5.17 and 5.19, eqn. 5.35 is written [24].

$$k = \frac{\rho_{s,a}}{M_{s,a}} \sum_{N_{age}=1}^{\infty} r_{N,age} \int_0^{t_{lim}} f_t k_s S_N \left( 1 - X_{carb}(t, N, C_{CO_2}^*) \right) dt \tag{5.35}$$

$k$  is the average kinetic constant whose the gas reacts, and it is the average of the different particles sorption capacity that the gas find in the reactor. Thus, now, it is also possible to use eqn. 5.28 and 5.29 to calculate the concentration of CO<sub>2</sub> exiting the reactor, using the gas-kinetic model.

## 5.5 Heat transfer model

In order to control the temperature in the reactor, or to use the available heat from the exothermic reaction, heat transfer surfaces are installed in which a proper heat transfer fluid flows. They can be of different types, vertical immersed tubes, horizontal immersed tubes, or also membrane walls, as it is used already in the

existing circulating fluidized bed combustors.

To predict the working temperature of the reactor, as well as the heat available, the heat transfer coefficient between the bed and the surfaces is needed. Since the heat transfer with membrane walls is the most studied case so far, due to the large use in combustors, also in this work membrane walls will be considered.

Heat transfer and hydrodynamics are strictly related, the motions of the gas and of the particles have a dominant role in the heat exchanged. A good heat transfer model, that predicts in a good way the real bed temperature, can not exist without an hydrodynamic model that is able to predict the particles motion in the reactor.

The main focus of the heat transfer model is the heat transfer coefficient,  $h$ , that relates the bed-wall heat transfer to the bed-wall temperature difference:

$$q = hA(T_{bed} - T_{wall}) \quad (5.36)$$

The heat transfer coefficient has a large number of variables from which it depends. It is observed that if the cross-sectional averaged solid density increases also  $h$  increases, as well as if the bed temperature increases, or if the particles diameter decreased. The length of the heat transfer surfaces influences  $h$ , if it increases,  $h$  decreases. If the bed diameter increases,  $h$  decreases, and finally also higher wall roughness can bring to higher value of  $h$ .

Heat transfer in circulating fluidized beds is composed by different contributions:

- *particle convection*, in which the particles, or cluster, exchange energy with the walls;
- *gas convection*, between gas motion and the walls;
- *radiation*, between the dense or dilute particles regions and the walls.

In fast fluidization regimes, the particles enhanced the heat transfer by an order of magnitude over single-phase gas flow in the same flow conditions [31], so a good physical understanding of the particle convection is fundamental.

Heat transfer models can be divided, in a first instance, in empirical models and mechanistic models. Empirical models try to find the most accurate fitting

of experimental data, having as output dimensionless variables related with operating conditions and design variables, in dimensionless terms. On the contrary, mechanistic models try to explain the experimental data relying on theoretical thoughts, and they come out with universal formulas as output. Basu and Nag in [32] divided further the mechanistic models, depending on how they calculate and explain the nature of the particle convection between the bed and the wall, and they can be classified in 3 groups: single-particle models, cluster renewal models and continuous film models. Fig 5.12 reports the classification of the heat transfer models.

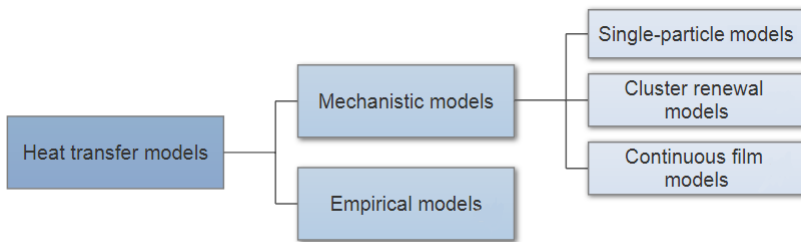


Figure 5.12: Classification of the heat transfer models

Since it is the most used and the most developed during the years, a particle renewal model will be used in this work to calculate the heat exchanged with the heat transfer surfaces.

### 5.5.1 Cluster renewal model

As already seen in Section 5.1.2, the cross-sectional structure of a fast fluidized bed can be divided in two regions in the radial direction: the annular, or wall, region and the core region. The temperature in the core region is near uniform [33], and can slightly decrease near the wall where heat transfer can take place. From the core region, clusters or particles are exchanged to the annular region, through a radial diffusion process. The annular region is not an homogeneous continuum with a solid concentration constant in time, as it has been depicted in the hydrodynamic and chemical kinetic model, to simplify the problem. Clusters formed, flow down for a certain distance and disintegrate, being replaced by dilute gas-solid mixture.

A schematic of this phenomenon is reported in Fig. 5.13.

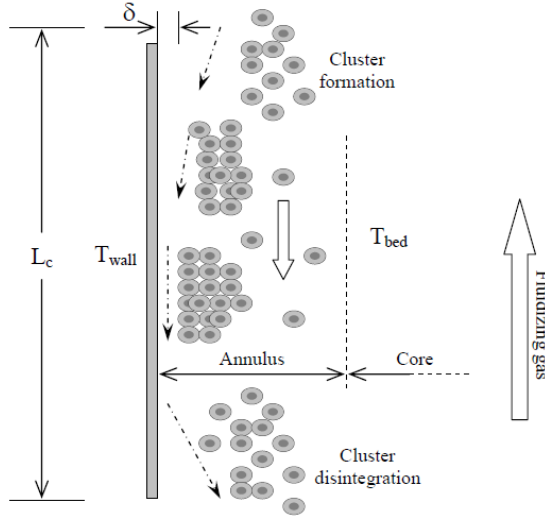


Figure 5.13: Representation of the cluster renewal model, (vijay and reddy 2005)

Mickley and Fairbaks in [34] have been the first who proposed the so called "cluster renewal model". According to this model, the cluster formed near the wall, during their permanence, exchanged heat with the wall, changing their temperature from the bed temperature, at which they are formed, to temperatures near the wall temperature, depending on the contact time. It can be deduced that the heat exchanged will change during their falling path till the clusters disintegrate, due to the presence of gas turbulence, and the particles go back to the core region. To model this phenomena what is proposed by Micley et al. is not to follow the temperature evolution of the cluster, but, assuming constant the temperature difference wall/cluster (cluster which is assumed to enter the wall region at the bed temperature), change the value of the cluster heat transfer coefficient during the permanence near the wall, an instantaneous heat transfer coefficient. It can be expressed as:

$$h_t = q(t)/(T_b - T_w) = \sqrt{\frac{k_c \rho_c c_c}{\pi t}} \quad (5.37)$$

and its mean value during the contact time will be:

$$\overline{h_t} = h_c = \sqrt{\frac{4k_c\rho_c c_c}{\pi t_c}} \quad (5.38)$$

where  $t_c$  is the contact time of the cluster.

The different cluster thermal properties ( $k_c$  and  $c_c$ ), and the cluster density, come from experimental relationships.

The main variable of a cluster is its solid fraction, that can be expressed using the relationship with the cross-sectional averaged voidage,  $\epsilon$  ( $= 1 - f$ , where  $f$  is one of the hydrodynamic outputs), given by eqn. (5.39) (from [35]):

$$c_{sf} = 1.23(1 - \epsilon)^{0.54} \quad (5.39)$$

Knowing the cluster solid fraction, and so the cluster voidage ( $\epsilon_c = 1 - c_{sf}$ ) cluster specific heat and cluster density, can be calculated weighting the properties of solid and gas:

$$c_c = (1 - \epsilon_c)c_{p,s} + \epsilon_c c_{p,g} \quad (5.40)$$

$$\rho_c = (1 - \epsilon_c)\rho_s + \epsilon_c \rho_g \quad (5.41)$$

It is different for the cluster thermal conductivity that is estimated from the empirical expression given by eqn. (5.42) (from [36])

$$k_c = k_g \left( 1 + \frac{(1 - \epsilon_c)(1 - k_p/k_g)}{k_g/k_p + 0.28\epsilon_c^{0.63(k_p/k_g)^{0.18}}} \right) \quad (5.42)$$

The average cluster contact time,  $t_c$  is another variable which is difficult to predict. It is generally calculated as:

$$t_c = \frac{L_c}{U_c} \quad (5.43)$$

where  $L_c$  is the contact length and  $U_c$  is the cluster falling velocity.

Wu et al. in [37], thanks to high speed cinematography, found a mean cluster falling velocity equal to 1.26 m/s, and give a relationship between the contact

length and the suspension density,  $\rho_{susp}$ :

$$L_c = 0.0178\rho_{susp}^{0.596} \quad (5.44)$$

where  $\rho_{susp}$  is the local suspension density, and it is calculated using a weighted average of the gas and solid density as:

$$\rho_{susp} = (1 - f)\rho_g + f\rho_s \quad (5.45)$$

Another aspect to take into account is that, different clusters can have different contact time with the wall, since the formation and the disintegration, is a random phenomenon driven by turbulence, and so eqn (5.38) should be also averaged for the difference clusters contact time. What is observed by Fang, in [38], is that the difference in  $h_c$  is not so high if it is averaged with respect the possible different cluster contact times, and so also in this work eqn. (5.38), the time-averaged heat transfer coefficient, will be adopted.

Besides the thermal resistance of the particle convection, there is a gas film resistance on the wall, due to an almost particle-free zone, with a thickness of the same order of the particles diameter, that increases if the particles are coarser. This resistance can be considered acting in series to the particle convection resistance [32]. It is expressed using the gas thermal conductivity and the dimensionless, experimental, gas layer thickness  $\delta$ , as reported in eqn (5.46).

$$h_w = \frac{k_g}{d_p\delta} \quad (5.46)$$

where  $\delta$  is given by [35]:

$$\delta = 0.0282(1 - \epsilon)^{-0.590} \quad (5.47)$$

Thus, the particle convection heat transfer coefficient is expressed as the series of the resistances, cluster thermal resistance and wall contact resistance:

$$h_p = \frac{1}{1/h_c + 1/h_w} \quad (5.48)$$

When the surface is not covered by clusters, it is exposed to a dilute solid-gas

phase, where the first heat transfer mechanism is the contact of the wall by the gas, which is almost at the bed temperature [33]. Wen and Miller in [39], from experimental studies in gas-solid transport lines, but also suitable for fluidized bed reactor applications, proposed the following correlation:

$$h_g = \frac{k_g c_{p,s}}{d_p c_{p,g}} \left( \frac{\rho_d}{\rho_s} \right)^{0.3} \left( \frac{u_t^2}{g d_p} \right)^{0.21} Pr \quad (5.49)$$

where  $\rho_d$  is the dilute phase density that depends on the solids fraction in the dilute phase Y, suggested equal to 0.001% by Basu in [40], and given by:

$$\rho_d = Y \rho_p + (1 - Y) \rho_g \quad (5.50)$$

At high bed temperature, radiation heat transfer from the bed to the wall becomes to be relevant. As also proposed by Vijay and Reddy in [41], the radiation heat transfer can be modelled considering the wall, the dense, and the dilute phases as grey parallel surfaces. The radiation heat transfer coefficient can be calculated for the two phases as:

$$h_{rc} = \frac{\sigma(T_{bed}^4 - T_w^4)}{(1/e_c + 1/e_w - 1)(T_{bed} - T_w)} \quad (5.51)$$

$$h_{rd} = \frac{\sigma(T_{bed}^4 - T_w^4)}{(1/e_d + 1/e_w - 1)(T_{bed} - T_w)} \quad (5.52)$$

where the cluster emissivity,  $e_c$ , can be calculated using the relationship proposed by Grace in [42]:

$$e_c = 0.5(1 + e_p) \quad (5.53)$$

where  $e_p$  is the emissivity of the particles. About the emissivity of the dilute phase, it can be calculated using the relationship given by Brewster in [43]:

$$e_d = \sqrt{\frac{e_p}{(1 - e_p)B} \left( \frac{e_p}{(1 - e_p)B} + 2 \right)} - \frac{e_p}{(1 - e_p)B} \quad (5.54)$$

where B is 0.5 in case of isotropic scattering.

All these heat transfer coefficients (particle convection, gas convection and radiation) are then combined together using the fraction wall coverage, the ratio of wall

surface covered by the cluster, which is related to the cross-sectional averaged solid suspension thanks to experimental equation proposed by Lint and Glicksmann in [35]:

$$f_{w,c} = 3.5(1 - \epsilon)^{0.37} \quad (5.55)$$

Thus, the final heat transfer coefficient is:

$$h_o = f_{w,c}(h_p + h_{rc}) + (1 - f_{w,c})(h_g + h_{rd}) \quad (5.56)$$

A typical profile of the local heat transfer coefficient is reported in Fig. 5.14.

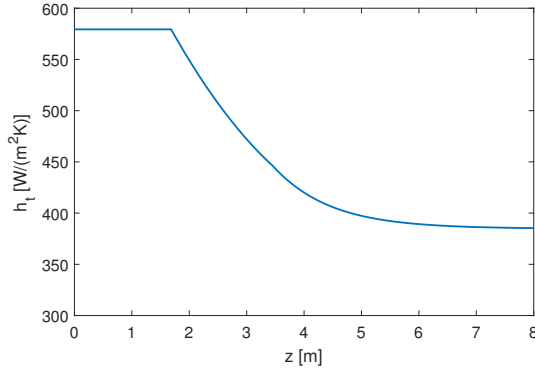


Figure 5.14: Typical values of the local heat transfer coefficient as a function of the height

### 5.5.2 Membrane walls and energy balance

The temperature inside the reactor can be considered uniform among gas phase and solid phase, due to the high gas velocity and the the small  $Bi$  number for particulates typically used in CFB reactors (much smaller than 0.1). This working temperature is also called bed temperature,  $T_{bed}$ .

To calculate the bed temperature, it is needed to know the temperature of the different mass flow rates, entering and exiting the reactor, the amount of  $\text{CO}_2$  captured by the particles, and the flux removed by heat transfer surfaces immersed in the reactor.

To remove energy from the reactor, membrane walls are considered. They consist of parallel tubes, connected longitudinally by fins or membrane bars, and in which an heat transfer fluid flows. They are insulated on one side and exposed to the gas-solid mixture on the other. They can be also used to contain the reactor. A representation is reported in Fig. 5.15.

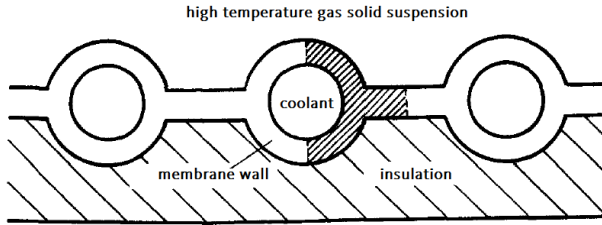


Figure 5.15: Representation of the cross section of the membrane wall used and of the portion analyzed (shaded) [23]

To compute the heat exchanged between the bed and the coolant a one-dimensional model is used for the global heat transfer coefficient bed/coolant. The assumptions adopted are:

- steady state conditions;
- isotropic properties of fins and tubes;
- 0 contact resistances at the junctions;
- uniform heat transfer coefficient tube/coolant and tube/bed;
- negligible fouling effect;
- adiabatic insulating side.

The membrane wall is characterized by the geometric parameters reported in Fig. 5.16, where  $\phi$  is the angle which subtends the base of the fin, and it is equal to:

$$\phi = 2\sin^{-1}(\beta) \quad (5.57)$$

with  $\beta = t/R_o$ , and  $\omega$  is the angle which subtends the portion of the tube exposed to the fluidized bed:

$$\omega = (\pi - \phi)/2 \quad (5.58)$$

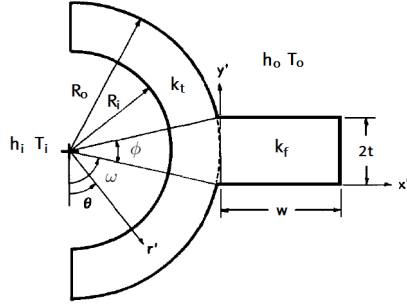


Figure 5.16: Membrane wall geometric parameters and heat transfer coefficients [23]

Heat transfer from the gas-particles mixture to the coolant has two possible ways: through the exposed tube surface and through the fin. Using an analogue electric circuit, these two possible paths can be treated as two one-dimensional resistors parallel connected. After these two, the heat is transferred radially inside the tube, through a thermal conductivity  $k_t$ , to the inner tube surface and finally to the coolant.

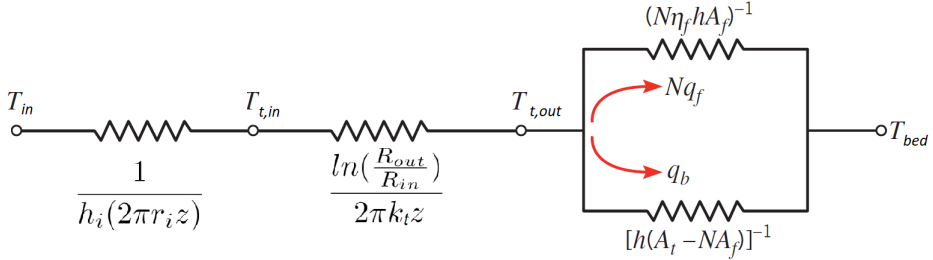


Figure 5.17: Equivalent thermal circuit for the heat transfer from the bed to the coolant

Thus, the thermal resistance bed/HTF can be expressed, as a function of the height  $z$ , as eqn. (5.59).

$$R_{tot}(z) = \frac{1}{h_i(2\pi r_i z)} + \frac{\ln(\frac{R_{out}}{R_{in}})}{2\pi k_t z} + \frac{1}{h_o(A_t(z) - N_{ext,fin}A_f(z)) + N_{ext,fin}\eta_f h_o A_f(z)} \quad (5.59)$$

If internal fins are used, in order to increase the internal heat transfer coefficient, the new equivalent thermal circuit takes into account the two new possible ways of

the heat transfer (free internal surface and internal fins surfaces) and it is reported in Fig. 5.18.

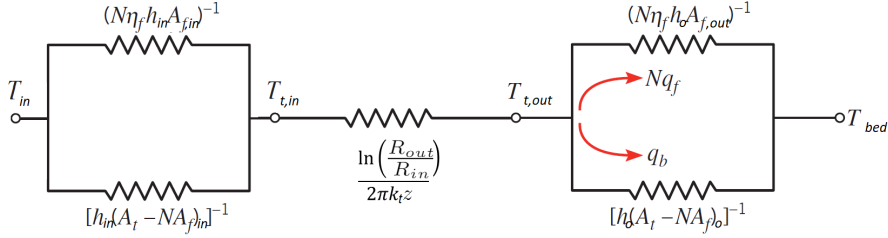


Figure 5.18: Equivalent thermal circuit with internal and external fins

The thermal resistance enhanced with the internal fins is equal to (5.60).

$$R_{tot}(z) = \frac{1}{h_i(A_{t,int}(z) - N_{int,fin}A_{f,int}(z)) + N_{int,fin}\eta_f h_i A_{f,int}(z)} + \frac{\ln\left(\frac{R_{out}}{R_{in}}\right)}{2\pi k_t z} + \frac{1}{h_o(A_{t,ext}(z) - N_{ext,fin}A_{f,ext}(z)) + N_{ext,fin}\eta_f h_o A_{f,ext}(z)} \quad (5.60)$$

Once that  $R_{tot}(z)$  is known, using the logarithmic mean value of the local heat transfer coefficient in the reactor, and assuming a constant heat transfer coefficient of the coolant,  $h_i$ , it is possible to calculate the outlet temperature of the coolant, as well as its behavior as a function of the height:

$$T_c(z) = T_{bed} - (T_{bed} - T_{c,in}) e^{-\frac{1}{m_c c_p (T_{c,out}) R_{tot}(z)}} \quad (5.61)$$

Thus, the total heat removed by the heat transfer fluid will be:

$$q_{out} = N_{tube} m_c c_p (T_{c,out}) (T_{c,out} - T_{c,in}) \quad (5.62)$$

Once  $q_{out}$  is known, applying an energy balance on the reactor (Fig. 5.19), knowing that the products leave the carbonator at the bed temperature, it is possible to

calculate the bed temperature as:

$$T_{bed} = \frac{\dot{m}_g c_{p,g,in} T_{g,in} + \dot{m}_s c_{p,s,in} T_{s,in} + \Delta H \dot{m}_g E_{CO_2} - q_{out}}{\dot{m}_g c_{p,g,out} + \dot{m}_s c_{p,s,out}} \quad (5.63)$$

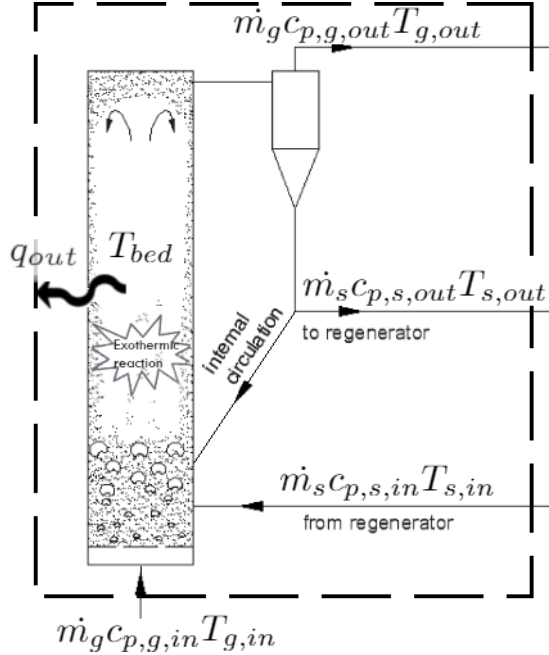


Figure 5.19: Energy balance applied on the carbonator reactor

## 5.6 Algorithm

All these concepts and formulas reported so far in this Section are implemented in Matlab, modelling the carbonator reactor in all its aspects. The flow chart in Fig. 5.20 represents the algorithm used, adapted from the algorithm proposed by Romano in [24] for a carbonator in a CaL-CO<sub>2</sub> capture process. It has to be highlighted that the main assumption of the model is the assumption of incompressible gas, so the concentration, or density, of the gasses will change only if there are adsorption phenomena.

Starting from the inner iteration process, this is used to compute the final capture efficiency of the reactor for the given input values. It is needed because the reaction rate constant,  $k$ , depends itself by the concentration of gases at which the particles are exposed during their residence time, and that is initially unknown.

First of all, since the level of partial carbonation,  $f_{carb}$ , is not known an iteration process is used to calculate also this variable, guessing an initial value, calculating  $X_{ave}$  and  $X_{max,ave}$  with eqn. (5.18) and (5.34), and so  $f_{carb}$  as  $X_{ave}/X_{max,ave}$ , till the guessed value and the calculated value are the same.

After that, guessing a starting value of equivalent  $\text{CO}_2$  ( $\text{CO}_2^*$ ) at which the particles are exposed in their the permanence time in the reactor, it is possible to calculate the reaction rate constant (using eqn. (5.35)), that will be considered uniform in the carbonator thanks to the perfectly mixed model used, and so the efficiency might be computed in two different ways, through the solid kinetic model, and through the gas kinetic model.

Using the solid kinetic model to express the capture efficiency, the average carbonation degree is the main variable. It is possible to write  $E_{\text{CO}_2}$  as:

$$E'_{\text{CO}_2} = \frac{F_R X_{ave}}{F_{\text{CO}_2}} \quad (5.64)$$

Whereas if the variation in  $\text{CO}_2$  concentration experienced by the gas flow rate is considered, the efficiency can be expressed using the gas flow rate in outlet as:

$$E''_{\text{CO}_2} = \frac{F_{\text{CO}_2,in} - F_{\text{CO}_2,out}}{F_{\text{CO}_2,in}} \quad (5.65)$$

This inner iteration process is repeated, changing the value of  $\text{CO}_2^*$ , average concentration whose the particles are exposed during their residence time, until the two efficiency values are the same. Furthermore

Another aspect to take into account, is the initial value of cross-sectional area and average molar mass of the solid, that depends on the particles carbonation degree, and so on the capture efficiency initially unknown. Guessing a initial value for  $A_t$  and  $M_s$ , they are adjusted when the capture efficiency is known. The new cross sectional area is calculated using the mean volumetric flow rate (eqn. (5.66)) in order to have a mean value of superficial gas velocity close to the desired one ( $u_0$ ), and the molar mass of the solid is adjusted using the average carbonation

of the particles, and weighting the molar mass of CaO and CaCO<sub>3</sub> for this value ( $X_{ave}$ ).

$$A'_t = \frac{(V_{g,in} + V_{g,out})/2}{u_0} \quad (5.66)$$

$$M'_s = (1 - X_{ave})M_{CaO} + X_{ave}M_{CaCO_3} \quad (5.67)$$

The last iteration process is related to the energy model applied. Again, since the carbonation behavior of the particles is a function of the concentration of CO<sub>2</sub> at which they are exposed, but also the CO<sub>2,eq</sub> changes if the temperature changes, an initial value of reactor temperature is guessed, calculating the capture efficiency, the energy released by the reaction and so the new reactor temperature, till the new temperature calculated converges to the final correct value.

The model implemented in Matlab is verified against the data published by Charitos in [44], for carbonators working in CO<sub>2</sub> capture, and the results are reported in Fig. 5.21, where in the x-axis there is the active space time, a variable which depends linearly by the average residence time,  $\tau$ , and the average carbonation degree of the particles in the reactor,  $X_{ave}$ , defined in [44].

In the case of the carbonator model applied to CaL-CSP, the variation of the volume flow rate is considered negligible, due to the fact that, as it will be shown in Section 6, the capture efficiency is lower than 10%, and so it is expected that the volume flow rate variation is a negligible effect, and so the variation of the mass flow rate of CO<sub>2</sub> is only attributed to the variation in concentration.

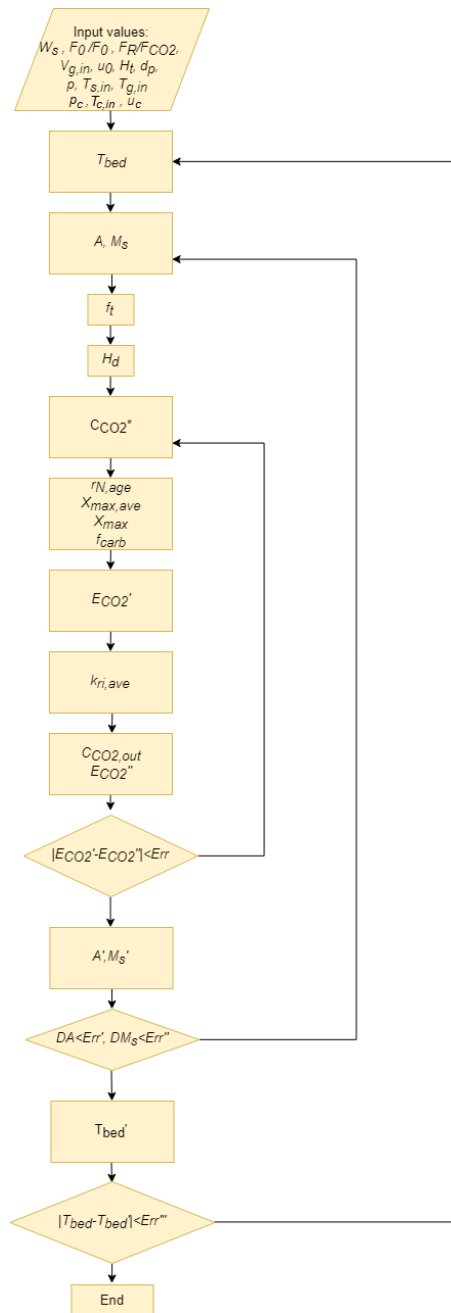


Figure 5.20: Flow chart of the carbonator model

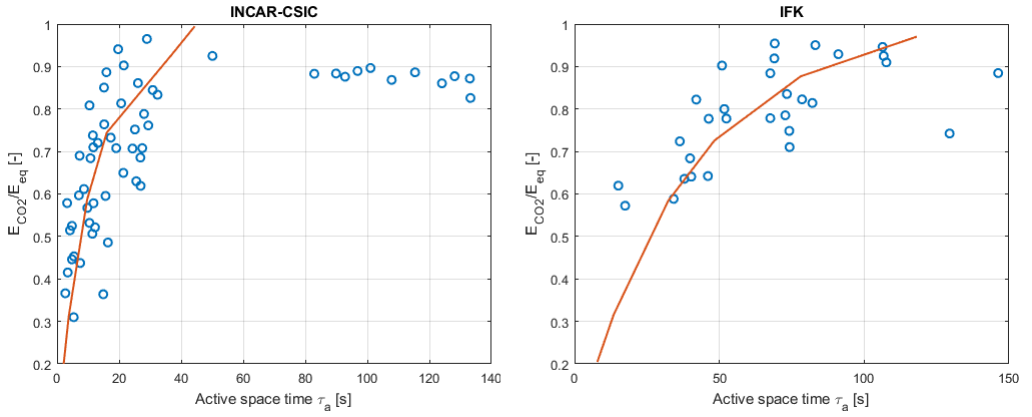


Figure 5.21: Output results from the model proposed by Romano in [24] compared with respect to the data from the INCAR-CSIC carbonator on the left, and with the data from IFK carbonator on the right [44]

# Chapter 6

## Data and results

In this chapter the parameters used to set the model and the results obtained are shown, analyzing how the reactor behaves with different operating conditions and design variables.

### 6.1 Reference design variables and operating conditions

The reference design variables and operating conditions are reported in table 6.1, taken from the study of Ortiz et. al in [45], where the CaL-CSP technology is studied, but without hydrodynamic and energy model and without planning membrane walls. In those conditions the bed temperature was 850°C working in fast fluidized regime.

The dimensions used for the membrane walls and for the fins are reported in table 6.2 and the cross sectional view of a tube which composes the membrane walls is reported in Fig. 6.2. An optimization study is carried out to choose the optimal dimensions of the internal fins, changing thickness ( $t_i$ ) and length ( $w_i$ ). Fig. 6.1 shows the variation of the extracted power as a function of the length of the internal fins for different thickness ( $t_i$ ), with  $u_c = 1m/s$  and  $Re_c < 2300$ , and it can be seen that the presence of the fins does not change appreciably the output power, and this variation would be even less if there was turbulent regime in the

Reactor operating conditions		Reactor design variables		Coolant operating conditions	
$p$	1 bar	$H_t$	36.67 m	$u_c$	3 m/s
$u_0$	4 m/s	$d_r$	8.89 m	$T_{c,in}$	650°C
$F_R/F_{CO_2}$	0.12			$p_c$	10 bar
$F_0/F_{CO_2}$	0				
$T_{s,in}$	703.17 °C				
$T_{g,in}$	725 °C				
$W_s$	200'000 kg				
$d_p$	40 nm				
$d_p^*$	0.92				
$u^*$	2.81				
CaO precursor	limestone				

Table 6.1: Reference operating conditions, reactor design variables and coolant operating conditions

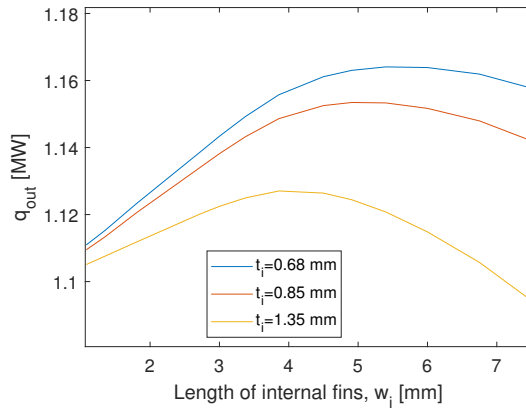


Figure 6.1: Results from the geometrical optimization of the internal fins, with  $Re$  of the coolant of  $\sim 2'000$

tubes (basically constant output power as a function of the internal fins length). As a consequence, the following results have been carried out using the optimum dimension found, but the final outputs from the model would not vary significantly if the internal fins contribution was neglected.

The final results using reference design variables and operating conditions are reported in Table 6.3. The power extracted, that will be used in a Stirling cycle, is

$R_i$	2.7 cm
$R_o$	3 cm
$\#internal\ fins$	12
$\#tubes$	349
$w_o$	0.5 cm
$t_o$	0.25 cm
$w_i$	0.54 cm
$t_i$	0.068 cm

Table 6.2: Dimensions of tube composing the membrane walls and of the internal and external fins (the variables referred to Fig. 6.2)

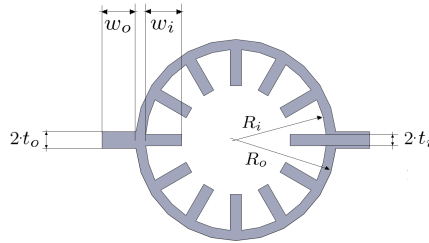


Figure 6.2: Cross-sectional view of the tube composing the membrane walls

around 9% of the energy released. This is a reasonable results since the reactor is initially designed as an adiabatic reactor, but anyway the power excreted could be easily increased in different ways discussed later on. The solid fraction as a function of  $z$  is reported in Fig. 6.3a, and the temperature profile of the coolant as a function of  $z$  in Fig. 6.3b, from which it can be seen how the coolant reaches rapidly the bed temperature, and so, if it was required, it would be possible to increase the extracted power increasing the coolant mass flow rate or decreasing the inlet temperature.

$H_d$	5.9 m	$E_{CO_2}$	6.4 %	$q_{gen}$	32.6 MW
		$f_{carb}$	0.9991	$q_{out}$	2.8 MW
		$X_{ave}$	0.53	$T_{bed}$	832.8°C

Table 6.3: Main results from the hydrodynamic, chemical and energy model with reference design variables and operating conditions

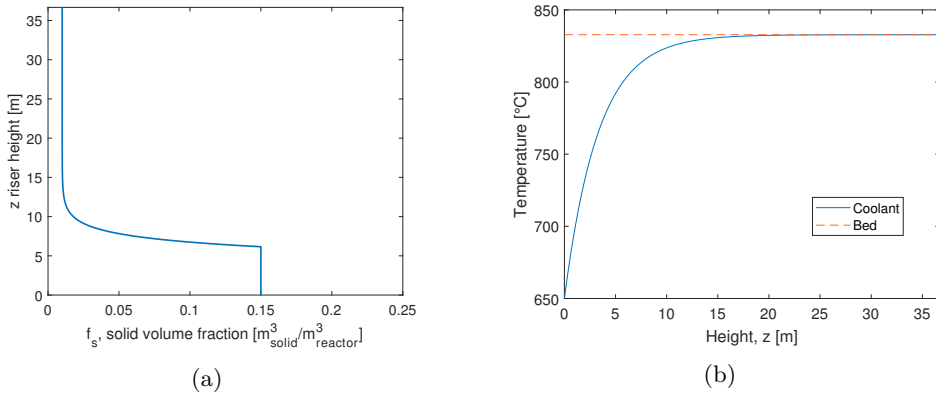


Figure 6.3: Solid fraction profile (a), temperature of the coolant as a function of  $z$  (b) using reference design variables and operating conditions

A scheme of the carbonator, with reference design variables and operating conditions, is reported in Fig. 6.4.

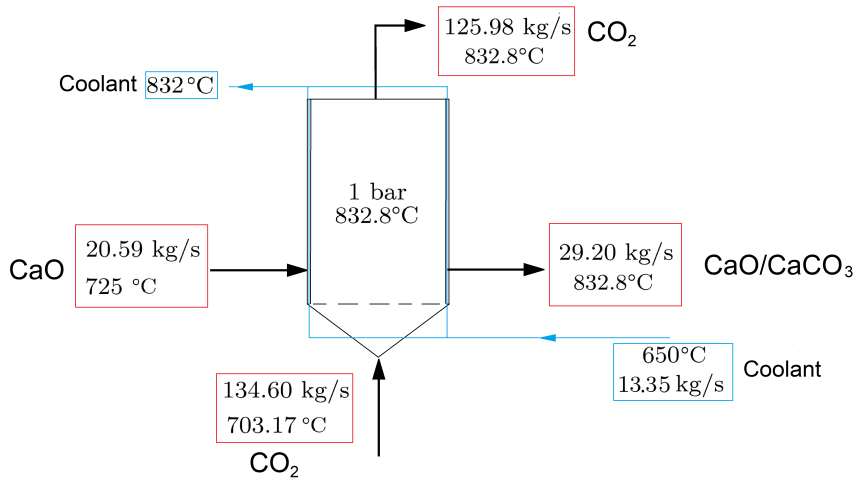


Figure 6.4: Carbonator scheme, using reference operating conditions and design variables

## 6.2 Analysis of the results for different input values

Thanks to the high CO<sub>2</sub> pressure used in a CaL-CSP storage technology, the sorbent particles reach their maximum carbonation degree,  $X_{max,N}$ , in few seconds (Fig 6.5a). Even if the CO<sub>2</sub> concentration changes, it is still far from the equilibrium condition, characteristic of CaL-CO<sub>2</sub> capture technologies (as it can be seen from Fig 6.5b), and so the limit time ( $t_{lim}$ ), needed to finish the fast reaction stage, will always be low enough to reach the particles maximum carbonation degree in the permanence time in the carbonator.

Thus, the dependency of the solid kinetic model with respect to the gas kinetic model is almost negligible, since basically the concentration is so high that its variation in the reactor height does not avoid to reach the end of the fast reaction stage to the particles, and so the gas-kinetic model can be neglected if the CO<sub>2</sub> concentration profile, as a function of the reactor height, is not needed. This observation leads to the conclusion that the parameter  $f_{carb}$ , that says how much the average carbonation level reached is different from the average maximum carbonation level, is almost equal to 1, as it is actually found in the simulations results. Indeed, it can be seen from Fig. 6.6, that only for values of the average residence time lower than around 30 s, the partial carbonation is not negligible, that means  $f_{carb} \lesssim 0.95$ , but for higher value of  $\tau$ , the value of  $X_{ave}$  could be considered equal to  $X_{max,ave}$ , and this happens in the reference case study where  $\tau \approx 500$ . Completely different is in the CO<sub>2</sub> capture carbonator, where the partial CO<sub>2</sub> pressure is less than 1 bar (usually around 0.2 bar) and so the residence time is much more important in order to reach values of  $f_{carb}$  close to 1, and in general also the dependency of the deactivation with respect to the partial carbonation must be taken into account using  $r_{n,age}$  (Section 5.2.1).

If the maximum carbonation level is always reached, the capture efficiency,  $E_{CO_2}$ , and so the energy released by the exothermic reaction is constant if the ratio  $F_R/F_{CO_2}$  is kept constant (eqn. (5.64)), or in other words the energy released is proportional to  $\frac{F_R}{F_{CO_2}}$ .

This conclusions will be fundamental to understand how, the changes in different variables (reactor geometry or operating conditions), will bring variations to

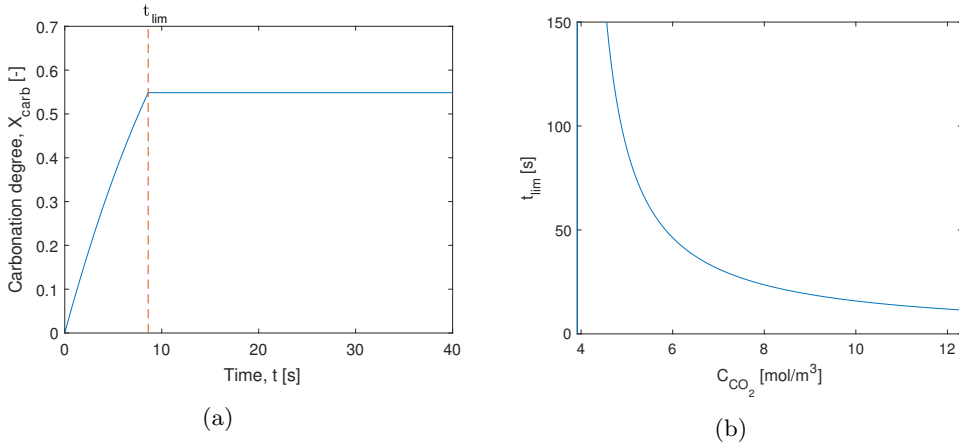


Figure 6.5: a) Sorbent carbonation degree ( $CO_2 = 11.24 \text{ mol/m}^3$ ,  $N = 100$ ), b) limit time as a function of  $C_{CO_2}$  ( $N=100, T_{bed} = 832 \text{ }^\circ\text{C}$ )

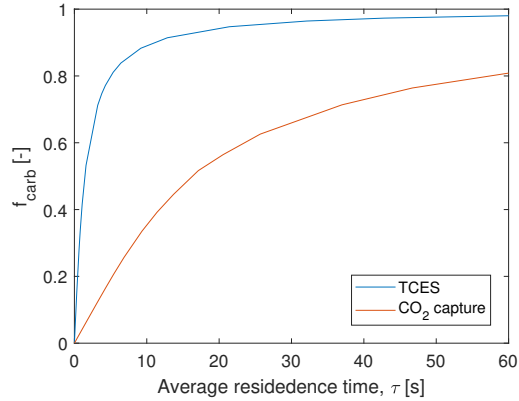


Figure 6.6: Partial carbonation as a function of different average residence times in the reactor for carbonator in TCES ( $p=1$  bar) and in  $CO_2$  capture plant ( $p_{CO_2}=0.2$  bar)

the output results.

### 6.2.1 Effect of diameter variation

In the design of the reactor the diameter is an important parameter since it will influence basically all the variables. If the reactor diameter varies, the hydrodynamic

of the particles and the heat transfer bed/coolant vary, whereas the chemical model has negligible variations due to the fact that the solid kinetic model is dominant. As it can be seen from Fig. 6.7a, if the reactor diameter increases, the height of the dense region decreases. As a consequence, the mean value of the heat transfer coefficient, fluidized bed side, decreases (Fig 6.7b), but this is also due to fact that the reactor temperature decreases (Fig. 6.8a), because the power extracted is higher (Fig. 6.8b) with larger diameter.

Since the gas volume flow rate is kept constant, and the reactor diameter increases, if  $\frac{F_R}{F_{CO_2}} = const$ , the capture efficiency and the energy released ( $q_{gen}$ ) are constant, since the moles of  $CO_2$  which have reacted are the same (same gas mass flow rate and same average carbonation degree of the particles,  $X_{ave}$ ). Instead, the increasing in the energy removed with the diameter, reported in Fig. 6.8b, is due to the increasing in the number of pipes installed in the membrane walls with the velocity of the coolant kept constant, so higher coolant mass flow rate, as it can be seen in Fig. 6.7b. About the bed temperature, Fig. 6.8a shows that decreases as the diameter increases, as it can also be deduced from Fig. 6.8b, because the power released is the same but the power extracted increases proportionally to the diameter.

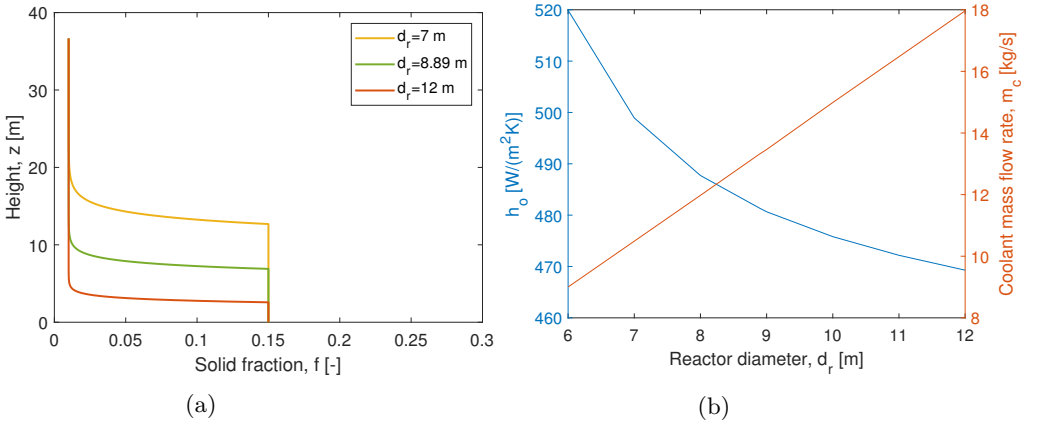


Figure 6.7: Solid fraction profiles for different reactor diameters (a), heat transfer coefficient, bed side, and total coolant mass flow rate for different reactor diameters (b)

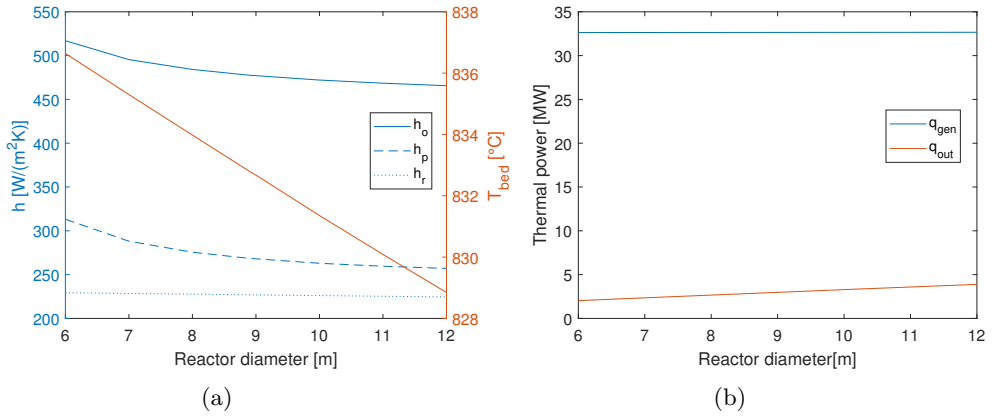


Figure 6.8: Logarithmic mean value of the local heat transfer coefficient in the reactor as a function of the reactor diameter (a), power released and power extracted as a function of the reactor diameter (b)

## 6.2.2 Effect of reactor total height variation

If the reactor height ( $H_t$ ) varies, again, the hydrodynamic will vary. As it can be seen from Fig. 6.9a, if the reactor height is increased, with constant solid inventory, the dense region height will decrease and as a consequence, also the mean value of the heat transfer coefficient, bed side. The power released does not change significantly, since even though the dense bed height varies, the solid kinetic model dominates on the gas kinetic model, and so the capture efficiency is kept constant. The power extracted keeps constant, since the coolant is always heated up till the bed temperature. If the coolant mass flow rate was higher, or if the inlet temperature was lower, the power extracted could change, but this is not the case.

About the bed temperature, as it can be seen from Fig. 6.9b, it does not change appreciably, since the capture efficiency keeps constant with the reactor total height, and extracted power keeps constant if the reactor height varies.

## 6.2.3 Effect of $F_R$ variation

As Fig. 6.10 shows, the dependency of the capture efficiency, and so, of the power generated, is almost linear as a function of  $\frac{F_R}{F_{CO_2}}$ , as it was expected since the exiting

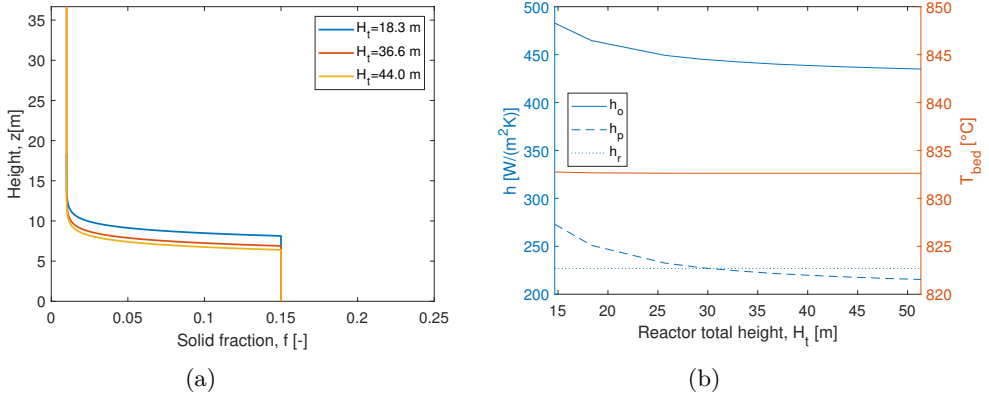


Figure 6.9: Solid fraction profiles for different reactor total height (a), Logarithmic mean value of the heat transfer coefficient, bed side, as a function of the reactor height (b)

sorbent carbonation degree is almost constant in  $\text{CO}_2$  pressure conditions of CaL-CSP storage, if the make-up flow does not change and if the average residence is kept constant. So, if  $F_R/F_{\text{CO}_2}$  increases, the bed temperature increases, and as a consequence the output power, since also the radiating term bed/coolant increases and the coolant reaches almost the bed temperature.

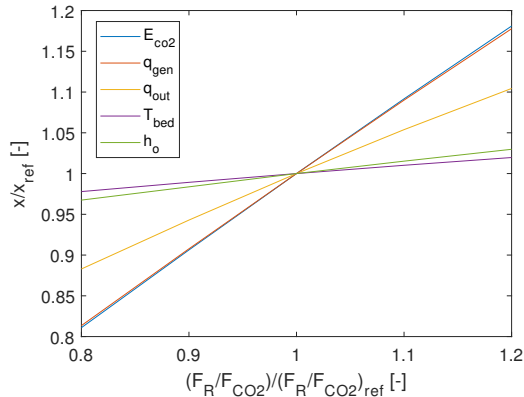


Figure 6.10: Sensitivity analysis of the carbonator model with respect to the variation of the recycling rate

### 6.2.4 Effect of $F_0$ variation

If a make-up mass flow,  $F_0$ , is planned, and so also a purge mass flow, the energy released by the reaction will be higher since the average maximum carbonation achievable will be higher (particles of first cycles are mixed with old particles). So, the trend expected if the make-up flow increases will be related to the one reported in Fig. 2.5. Fig. 6.11a shows the results from the simulation, using the reference design variables and operating conditions, and it can be seen how the power released reaches an asymptotic value if  $F_0$  increases. Furthermore, the bed temperature will increase because the coolant operating conditions, inlet temperature, velocity and pressure, are kept as the reference ones. The same is for the value of the average carbonation degree of the particles in the carbonator ( $X_{ave}$ ) that, as expected, increases if the make-up flow increases, since there are more particles with higher maximum carbonation degree achievable (Fig. 6.12).

There is a limit for the make-up flow, above which the reactor temperature exceed the equilibrium temperature, and so above which it is not desirable to go. For example if  $p = 1$  bar the make-up flow can not exceed 7 t/h (Fig. 6.12).

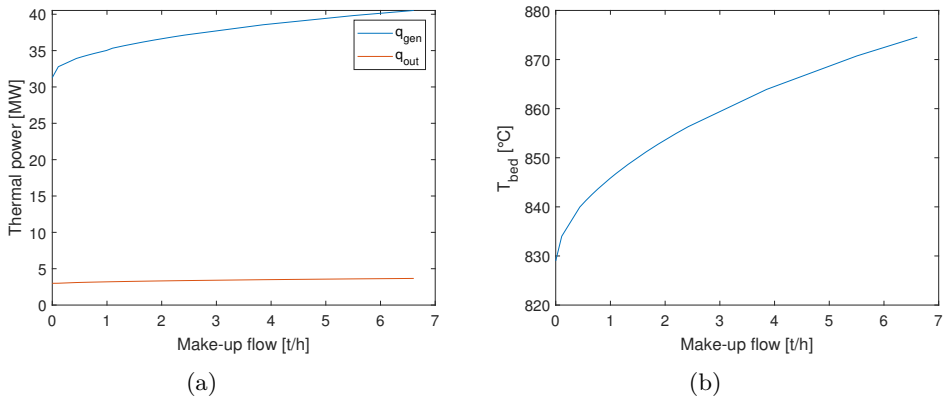


Figure 6.11: Power released and extracted as a function of the make-up flow in the carbonator (a), bed temperature as a function of the make-up flow (b) with reference design variables and operating conditions

If the reactor pressure increases the limiting make-up flow increases, and so the average carbonation degree increases, as it can be seen from Fig. 6.13, and

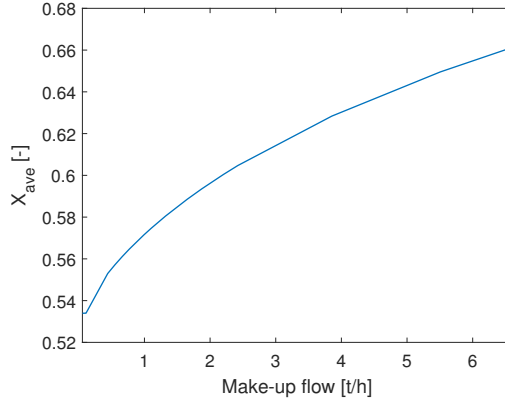


Figure 6.12: Average carbonation degree of the particles in the carbonator as a function of the make-up flow

so the power released and the bed temperature will increase as well (Fig. 6.14a and 6.14b), the power extracted will be almost constant if the coolant operating conditions (inlet temperature, pressure and velocity) are kept constant.

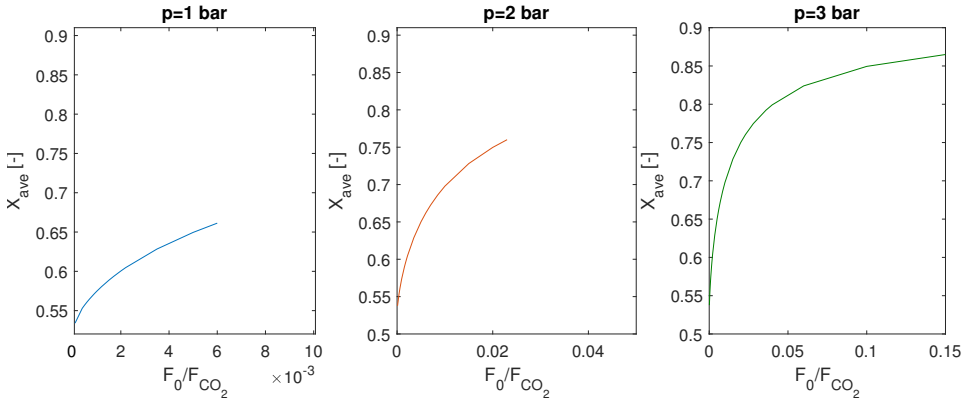


Figure 6.13: Average carbonation degree of the particles in the carbonator as a function of the make-up flow, using reference design variables and operating conditions, with pressure of the reactor equal to 1, 2 and 3 bar

It has to be noted in Fig. 6.14a, same values of  $F_0/F_{CO_2}$  give different value of  $T_{bed}$  for different pressure. This is because even if  $F_0/F_{CO_2}$  is the same, since

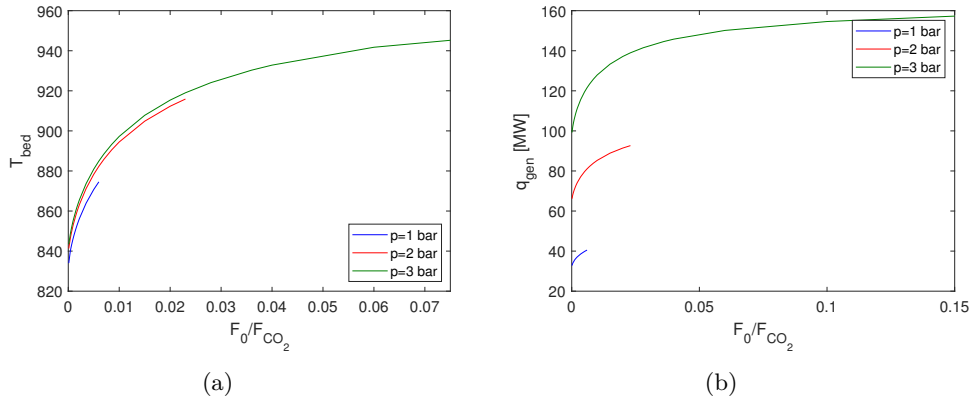


Figure 6.14: Bed temperature (a) and power released by the exothermic reaction (b) as a function of the ratio  $F_0/F_{CO_2}$

the reactor pressure is higher, also the pressure of the gas flow rate ( $F_{CO_2}$ ) will be higher, and so in absolute terms,  $F_0$ , that is equal to  $\frac{F_0}{F_{CO_2}} \cdot F_{CO_2}$  will be higher for higher pressure, and as a consequence the bed temperature as well.

# Chapter 7

## Conclusions

Starting from a carbonator model applied to a CaL-CO<sub>2</sub> capture plant, it has been possible to make a model adjusted for the use of the calcium-loop as a TCES, characterized by its different characteristic operating conditions.

The model used is really reliable from the chemical point of view since adjusted from carbonator model used for CO<sub>2</sub> capture, where small variations in gas concentration and solid carbonation degree mean great variations in the capture efficiency, differently in a CaL-CSP plant, where the pressure is so high that some phenomena could be also neglected (such as the partial carbonation effect). So, the capture efficiency, and the energy released are computed in a detailed way.

Once that the energy available from the reaction has been computed, the possibility to install membrane walls has been taken into account. As it can be seen from the results reported in Section 6, the energy extracted by the coolant is high enough to promote the use of a Stirling cycle, which would use the power extracted from the reactor to work, and that ideally could have higher performance than Joule-Brayton cycles. Furthermore the use of a coolant can help the control of the temperature of the reactor which must not reach temperature that are too high, that could increase the deactivation phenomena whose the sorbent is subjected.

The possibility to use a make-up flow is also studied. The results show that a make-up flow can increase a lot the performance of the reactor keeping constant the recycling mass flow rate, and so it has been found out that this is another

possibility to control the output power.

The carbonator model introduced in this work could be easily implemented in a model of the plant, in order to understand the best operating conditions, that will be related with how the other components work, in particular the availability of energy during the day, the volume and the pressure of the storages, and the energy market demand to fulfill.

Furthermore from the results obtained, suggestions for further works could be to study the hydrodynamic model more in detail, maybe with a CFD model, since in this work a semi-empirical model is used (even though it gives reliable predictions), and it would be also advisable to adjust the plug flow model used for the gas phase, in order to take into account the volume flow rate variation when the capture efficiency exceed 10%.

# Bibliography

- [1] N'Tsoukpoe K., Liu H., Le Pierrée N, Lou L., 2009. *A review in long term sorption solar energy storage*, Renew Sust Energy Rev.
- [2] Kyaw K., Matsuda H., Hasatani M., 1996. *Applicability of carbonation/decarbonation reactions to high-temperature thermal energy storage and temperature upgrading*, J Chem Eng Jpn.
- [3] Martínez I., Grasa G., Parkkinen J., Tynjälä T., Hyppänen T., Murillo M, Romano M.C., 2016. *Review and research needs of Ca-Looping systems modelling for post-combustion CO<sub>2</sub> capture applications*, International Journal of Greenhouse Gas Control 50,271–304
- [4] Levenspiel D., Kunii O.,1991. *Fluidization Engineering*, second ed., Butterworth-Heinemann, Newton, MA, USA.
- [5] Alvarez, D., Abanades, J.C., 2005. *Determination of the critical product layer thickness in the reaction of CaO with CO<sub>2</sub>*, in Ind. Eng. Chem. Resour. 44, 5608–5615.
- [6] Muschelknautz E. and Greif V., 1997. *Cyclones and other gas-solids separators*, in *Circulating fluidized bed* edited by J.R. Grace, A.A. Avidan and T. M. Knowlton.
- [7] M. Benitez-Guerrero M., Sarrion B., Perejon A., Pedro E. Sanchez-Jimenez R., Perez-Maqueda L.A., Valverde J. M., 2017. *Large-scale high-temperature solar energy storage using natural minerals*, in Solar Energy Materials and Solar Cells 168, 14–21.
- [8] C. Ortiz, R. Chacartegui, J.M. Valverde, J.A. Becerra, L.A. Perez-Maqueda, 2015. *A new model of the carbonator reactor in the calcium looping technology for post-combustion CO<sub>2</sub> capture*, in Fuel 160, 328–338.

- [9] Dieter H., Charitos A., Bidwe A. R., Wei A., Zieba M., 2011. *Study of Standpipe and Loop Seal Behavior in a Circulating Fluidized Bed for Geldart B Particles*, in 10th International Conference on Circulating Fluidized Beds and Fluidization Technology - CFB-10.
- [10] D. Geldart, 1973. *Types of gas fluidization*, Powder Technology, 7, pp 285-292.
- [11] J. R. Grace, 1986. *Contacting Modes and Behaviour Classification of Gas-Solid and Other Two-Phase Suspension*, Canadian Journal of Chemical Engineering, 64, 353 .
- [12] Li Y., Kwauk M., 1980. *The dynamic of fast fluidization*, in Fluidization III, Plenum Press, New York.
- [13] Lasheras A., Ströhle J., Galloy A., Epple B., 2011. *Carbonate looping process simulation using a 1D fluidized bed model for the carbonator*, in International Journal of Greenhouse Gas Control 5 686–693.
- [14] R. Chacartegui, A. Alovísio, C. Ortiz, J.M. Valverde, V. Verda, J.A. Becerra, 2016. *Thermochemical energy storage of concentrated solar power by integration of the calcium looping process and a CO<sub>2</sub> power cycle*, in Applied Energy 173 589–605.
- [15] H. Scott Fogler, 2010. *Essential of Chemical Reactor Engineering*, Pearson Education, Boston.
- [16] Pugsley T. S., Berutti F., 1996. *A predictive hydrodynamic model for circulating fluidized bed risers*, in Powder Technology, 89, pp 57-69.
- [17] H. Weinstein et al., 1983. in Fluidization TV, D. Kunii and R. Toei, eds., p. 299, Engineering Foundation, New York, 1983; AIChE Symp. Ser.
- [18] L. Monceaux et al., in Circulating Fluidized Bed Technology, P. Basu, ed., p. 185, Pergamon, New York, 1986.
- [19] Sarrion B., Valverde J. M., Perejon A., Perez-Maqueda L., and Sanchez-Jimenez P. E., 2016. *On the Multicycle Activity of Natural Limestone/Dolomite for Thermochemical Energy Storage of Concentrated Solar Power*, in Energy Technol. 2016, 4, 1013 – 1019.
- [20] Hartge, Y Li, and J. Werther, in Circulating Fluidized Bed Technology, P. Basu, ed., p. 153, Pergamon, New York, 1986.
- [21] Kunii D. and Levenspiel O., 1997. *Circulating fluidized-bed reactors*, in Chemical Engineerin 9 Science, Vol. 52, No. 15, pp. 2471-2482.

- [22] Kunii D. and Levenspiel O., 2000. *The K-L reactor model for circulating fluidized beds*, in Chemical Engineering Science 55, 4563-4570.
- [23] B. D. Bowen, M. Fournier and R. Grace, 1991. *Heat transfer in membrane waterwalls*, in Int. J. Heat Mass Transfer, 34,1043–1057.
- [24] Romano C. M., 2012. *Modeling the carbonator of a Ca-looping process for CO<sub>2</sub> capture from power plant flue gas*, in Chemical Engineering Science, 69,257–269.
- [25] Grasa G., and Abanades J. C., 2006. *CO<sub>2</sub> Capture Capacity of CaO in Long Series of Carbonation/Calcination Cycles*, in Ind. Eng. Chem. Res. 2006, 45, 8846-8851.
- [26] Abanades J. C., 2002. *The maximum capture efficiency of CO<sub>2</sub> using a carbonation/calcination cycle of CaO/CaCO<sub>3</sub>*, in Chemical Engineering Journal 90, 303–306.
- [27] Grasa G., Abanades J. C., and Anthony E. J., 2009. *Effect of Partial Carbonation on the Cyclic CaO Carbonation Reaction*, in Ind. Eng. Chem. Res., 48, 9090–9096.
- [28] N. Rodríguez, M. Alonso, J.C. Abanades, 2010. *Average activity of CaO particles in a calcium looping system*, in Chemical Engineering Journal 156, 388–394.
- [29] García-Labiano F., Abad, A., de Diego L.F., Gayan P., Adanez J., 2002. *Calcination of calcium based sorbents at pressure in a broad range of CO<sub>2</sub> concentrations*, in Chem. Eng. Sci. 57, 2381–2393.
- [30] Gemma S. Grasa, J. Carlos Abanades, Monica Alonso, Belen Gonzalez, 2008. *Reactivity of highly cycled particles of CaO in a carbonation/calcination loop*, in Chemical Engineering Journal 137, 561–567.
- [31] J. R. Grace, A. A. Avidan, T. M. Knowlton, 1997. *Circulating fluidized bed*, 1st edition, Chapman Hall.
- [32] P. Basu, P. K. Nag, 1995. *Heat transfer to walls of a circulating fluidized-bed furnace*, in Chemical Engineering Science 51, 1-26.
- [33] Yerushalmi J., David H. Turner, Arthur M. Squires, 1975. *The fast fluidized bed*, in Ind. Eng. Chem., Vol. 15, 47-53.
- [34] Joseph Yerushalmi, Mickley, H.S., and D.F. Fairbanks, 1955. *Mechanism of heat transfer to fluidized beds*, in AIChE Journal 1, 374-384.
- [35] Lints, MC., and L.R. Glicksman, 1994. *Parameters governing particle to wall heat transfer in a circulating fluidized bed*, in A.A. Avidan, (Ed.), Circulating

- Fluidized Bed Technology, AIChE, New York, IV, pp. 63-82.
- [36] Gelperin, N.I., and V.G. Einstein, 1971. *Heat transfer in fluidized beds*, in J.F. Davidson, D. Harrison (Eds.), *Fluidization*, Academic Press, London, pp. 471-540.
- [37] R. L. Wu, C. J. Lim, J. R. Grace, C. M. H. Brereton, 1991. *Instantaneous Local heat transfer and hydrodynamics in a circulating fluidized bed*, in Int. J. Heat Mass Transfer. Vol. 34. No. 8, pp. 2019-2027.
- [38] Z. H. Fang, J. R. Graces and C. J. Lim, 1995. *Local particle convective heat transfer along surfaces in circulating fluidized beds*, in Int. J. Heat Mass Transfer. Vol. 38, No. 7, pp. 1217-1224.
- [39] Chin-Yung Wen and Eugen N. Miller, 1961. *Heat Transfer in Solids-Gas Transport Lines*, in *Industrial and Engineering Chemistry* 53, 51-53.
- [40] Basu P., 1990. *Heat transfer in fast fluidized bed combustors*, in *Chemical Engineering Science* 45, 3123-3136.
- [41] G. Nirmal Vijay and B. V. Reddy, 2005. *Effect of Dilute and Dense Phase Conditions on Bed-to-Wall Heat Transfer Mechanism in the Riser Column of a Circulating Fluidized Bed Combustor*, in *Proceedings of FBC2005, 18th International Conference on Fluidized Bed Combustion*.
- [42] Grace, J.R., 1982. *Fluidized bed heat transfer*, in G. Hestroni, (Ed.), *Handbook of Multiphase Flow*, McGraw-Hill, Hemisphere, Washington, D.C., pp. 9-70.
- [43] Brewster, M.Q., 1986. *Effective absorptivity and emissivity of particulate sender with application to a fluidized bed*, in *Transactions of the ASME* 108, 710-713.
- [44] Alexander Charitos, Nuria Rodríguez, Craig Hawthorne, Monica Alonso, Mariusz Zieba, Borja Arias, Georgios Kopanakis, Gunter Scheffknecht, and Juan Carlos Abanades, 2011. *Experimental Validation of the Calcium Looping CO<sub>2</sub> Capture Process with Two Circulating Fluidized Bed Carbonator Reactors*, in *Ind. Eng. Chem. Res.* 2011, 50, 9685-9695.
- [45] C. Ortiz, J. M. Valverde, R. Chacartegui, and L. A. Perez-Maqueda, 2018. *Carbonation of Limestone Derived CaO for Thermochemical Energy Storage: From Kinetics to Process Integration in Concentrating Solar Plants*, in *ACS Sustainable Chem. Eng.* 2018, 6, 64046417.